Journal of Structural Geology 182 (2024) 105114

Contents lists available at ScienceDirect

Journal of Structural Geology

journal homepage: www.elsevier.com/locate/jsg

Matrix deformation of marls in a foreland fold-and-thrust belt: The example of the eastern Jaca basin, southern Pyrenees

R.L. Menzer [a,*], C. Bonnel [a], F. Gracia-Puzo [a,b], C. Aubourg [a]

[a] Laboratoire des Fluides Complexes et Leur Réservoirs, UMR 5150 Université de Pau et des Pays de L'Adour – CNRS, Pau, France
[b] Geotransfer Research Group (IUCA), Universidad de Zaragoza, Spain

ARTICLE INFO

Keywords:
Marls
Magnetic fabric
Matrix deformation
Strain gradient
Jaca basin
Southern pyrenees

ABSTRACT

In this study, we used the Anisotropy of Magnetic Susceptibility (AMS) to investigate the matrix strain record of two calcareous shale formations, the Eocene Larrès and Pamplona Marls, along the eastern Jaca foreland fold-and-thrust belt (Southern Pyrenees). More than 1000 unoriented fragments, collected from 62 sites along 4 sub-parallel sections in the footwall of the regional Oturia thrust and through local Yebra anticline, were measured. The analysis of the degree of anisotropy (P') and shape parameter (T) allowed to identify four types of magnetic fabrics. Type II fabrics associated with poorly deformed rocks are characterized by a relatively high anisotropy and an oblate shape. In contrast, type III fabrics, associated with strongly fractured rocks are characterized by the lowest anisotropy and a triaxial shape. Type IV and type V fabrics are characterized by increasing anisotropy and shape parameters, and are associated with the development of a weak to a slaty cleavage in rocks. The distribution of the magnetic fabric is roughly similar along the four studied sections. In the footwall of the Oturia thrust, magnetic fabrics evolve from the type V to type II over a 1000 m-long interval. By contrast, the distribution of magnetic fabric is roughly symmetric across the Yebra anticline, evolving from a dominating type II fabric in both limbs to mixed type III-type V fabrics within the 1 km-large hinge zone. The succession of the magnetic fabrics is interpreted as recording various degrees of matrix strain in response to thrusting and folding. The correlation of magnetic fabrics between the four sections highlights some along-strike variations in the extension of fabric domains that are interpreted as reflecting the local influence of 2nd-order factors, such as the syn-tectonic sedimentation. Results are integrated within the tectono-sedimentary framework of the studied area to propose a model of matrix strain related to the tectonic and sedimentary evolution of a foreland fold and thrust belt.

1. Introduction

Fold-and-Thrust Belts (FTBs) are the main macro-scale structures that develop in foreland basins in response to the regional shortening during the growth of orogenic wedges (Dahlen et al., 1984; Davis et al., 1983). FTBs classically propagate in-sequence from the inner zones toward the foreland although out-of-sequence and backward-verging thrusts can develop in response to forcing parameters. The development of FTBs is expressed by the emplacement of thrust-sheets as well as fault-related folds in the sedimentary cover (Brandes and Tanner, 2014; DeCelles and Giles, 1996). The deformation is recorded by wedge-shaped progressive unconformities and growth strata within the sedimentary filling and is accompanied by the mesoscale deformation of involved rocks, including the development of fractures networks, joints and calcite veins (Tavani et al., 2015). Based on these tectono-sedimentary markers, authors classically recognized three main stages during folding (Lacombe et al., 2021). First is a Layer Parallel Shortening (LPS) stage during which the horizontal compressive stresses are accommodated by the development of micro- and meso-scale structures within the pre-growth strata. Then the ongoing shortening results in the macro-scale curvature of the sedimentary strata the main folding event that is accommodated both by flexural slip in the folds limbs and tangential-longitudinal strain along the fold hinge (Pueyo-Morer et al., 1997). The fold growth stops when the tilting of limbs is no longer sufficient to accommodate the horizontal shortening, which is finally transferred to the flattening of the fold hinge during the Late Stage Fold Tightening (LSFT).

Propagation of FTBs is mainly controlled by mechanical properties of

* Corresponding author. Université de Pau et des Pays de l'Adour, Avenue de l'Université, 64000 Pau, France.
E-mail address: rl.menzer@univ-pau.fr (R.L. Menzer).

https://doi.org/10.1016/j.jsg.2024.105114
Received 12 September 2023; Received in revised form 18 March 2024; Accepted 18 March 2024
Available online 23 March 2024

the wedge, and basal fault and topographic surface dips. In this context, the propagation and tectonic evolution of FTBs are partly controlled by the nature and rate of the syn-orogenic sedimentation, both at the local scale of the structure (Barrier et al., 2002, 2013; Nalpas et al., 2003; Pichot and Nalpas, 2009) and at the regional scale (Duerto and McClay, 2009; Fillon et al., 2013a). First, the deposition of low-strength lithologies such as salt and shales in front of orogenic belt during the foreland infilling can lead to complex tectonics styles during the subsequent deformation of the basin, as expressed by the propagation of thin-skinned thrust-sheets, the initiation of local diapirism and/or the development of passive-roof duplex and break-back thrusts (Davis and Engelder, 1985; Duerto and McClay, 2011; Kergaravat et al., 2017). Second, the rate of syn-tectonic sedimentation strongly influences the geometry and the growth of contractional structures as well as the structural style and the extension of thrust-sheets and fold belts (Duerto and McClay, 2009; Fillon et al., 2013).

The sedimentary environments evolution in FTBs during the propagation of the lithosphere flexure and the increased of regional dynamic subsidence is linked to the migrating depozones (DeCelles and Giles, 1996). Nevertheless, within foreland basins during the early stages of the basin filling, fine-grained and low-strength lithologies, such as marls and shales, may form the dominant sedimentary units, when high subsidence conditions result in the drowning of the forebulge (Sinclair, 1997). These syn-orogenic marine shales has been recognized as intermediates or major decollement levels in some of the well-described FTBs around the world (Chapman and DeCelles, 2015), among which are the Himalayan Main Frontal Thrust (DeCelles et al., 1998, 2001) and the Eastern Bolivian Cordillera in central Andes (McQuarrie, 2002; McQuarrie and DeCelles, 2001). Furthermore, shales undergone several physical transformations during burial that greatly modify their mechanical behaviour and is leading to complex, localized and evolutive deformations patterns (Soto et al., 2021a, 2021b). In particular, the dewatering of clay particles during diagenetic smectite-illite transformation, as well as the hydrocarbon generation during the maturation of the organic matter, are responsible both for the strong increase in pore pressure within shales units. If insufficiently drained, for example in a context of high sedimentation rates, this can lead to overpressured shales in which the clay matrix will undergo a visco-platic deformation. This singular mechanical behaviour results in various successive shales tectonics processes beginning with the initiation of intra-formational detachments and the early growth of shale-related folds (Deville et al., 2020; Morley et al., 2017, 2018). It can be followed in some cases by the passive growth of shales walls and diapirs in a salt-like, ductile mobile shales tectonics (Morley, 2003; Morley et al., 1998; Soto et al., 2010). In some ultimate cases, the complete fluidization of shales and the piercement of shales structures lead to the spreading of mud volcanoes and shale sheets on the basin floor (Blouin et al., 2020; Hudec and Soto, 2021; Soto and Hudec, 2023).

Characterizing the matrix deformation of shales is therefore essential to unravel tectonics processes in a shale-rich foreland fold-and-thrust belts as well as the effect of the syn-tectonic sedimentation. In shale rocks with a high fraction of clay particles (>30%), such as marls, silts and claystones, the magnetic fabric remains one of the most effective proxy to describe the bulk preferential orientation of the clay matrix (Borradaile and Henry, 1997; Hrouda, 1982; Tarling and Hrouda, 1993). The magnetic fabric can be quickly estimated by measuring the Anisotropy of Magnetic Susceptibility, represented in space by an ellipsoid defined with the magnitudes and orientations of the Kmax $\geq$ Kint $\geq$ Kmin principal susceptibilities axes, that reflect the organisation of the clay petrofabric. Since the pioneering work in compressive domains (Aubourg et al., 1991; Averbuch et al., 1992; Kissel et al., 1986) and extensive domains (Cifelli et al., 2005), it has been observed that this technique is highly sensitive to characterize the matrix deformation in weakly deformed mudrocks and has made the technique widely used FTBs (Cifelli et al., 2004; Parés et al., 1999).

In this work, we propose therefore to use the AMS method to characterize the clay fabric and to decipher the matrix deformation of shales along a shale-rich FTB, with the aim to highlight the deformation mechanisms as well as the influence of the syn-tectonic sedimentation.

In southern Pyrenees, the Jaca foreland basin appears as a world-class area to answer these questions. At the transition between the northern turbiditic and the southern molassic sub-basins, a narrow, 10 km large zone contains three shale-cored folds detached within the Eocene marls. Each of these detachment folds is spatially associated with alluvial fan conglomerates in its backlimb. Growth strata and progressive unconformities within these deposits suggest a strong relationship between synchronous folding and sedimentation processes.

2. Geological setting

2.1. Structural framework of the jaca basin

The Jaca basin, 50 km wide and 150 km long, is located in the west-central part of the South Pyrenean fold-and-thrust belt (Fig. 1A), which developed in response to the continental collision between Eurasian and Iberian plates from Late Cretaceous to Miocene times (Ford et al., 2022; Teixell et al., 2016; Vergés et al., 2002). During the Palaeocene-Eocene, the Jaca basin was the main peripheral foreland basin filled with orogen-derived sediments, before it evolved as a southward-carried piggy-back basin during Oligocene (Hogan and Burbank, 1996; Ori and Friend, 1984).

The Jaca basin can be divided from north to south in three structural units that correspond to the successive migrating foreland depocenter (Fig. 1B). To the north, the Hecho turbiditic basin corresponds to a 4 km-thick unit of lower and middle Eocene turbidites deposited in the early-orogenic foredeep depozone (Labaume et al., 1985; Remacha and Fernández, 2003). The central part of the basin corresponds to a 100 km-long, low-topography area that is dominated by shallow-marine marls and deltaic sandstones formations. The marls units form especially the narrow hinge zone of three, small-extension (10 km) and short-wavelength (1–5 km) growth anticlines (Millan Garrido et al., 2006; Teixell, 1996). Each are associated with a local depositional syncline filled by alluvial fan conglomerates (Montes and Colombo, 1996; Montes Santiago, 2009; Roigé et al., 2017). To the south, the Guarga molassic basin corresponds to a 3,5 km-thick unit of late Eocene – Oligocene continental deposits filling the 20 km-large, E-W trending, Guarga synclinorium (Montes Santiago, 2009; Puigdefábregas, 1975).

These different basins are characterized by various structural styles and decollement levels. The northern turbiditic basin is deformed as N110°-trending minor thrusts and fault-related folds. These structures developed in response to the emplacement of the Monte Perdido and Larra thrust systems which are both detached at the base of the 750 m-thick Upper Cretaceous (Labaume et al., 1985). These structures are located on the hanging-wall culmination of the Gavarnie thrust-sheet and therefore can only be related to the Eaux-Chaudes thrusting during Lutetien and Bartonian times (Labaume et al., 2016).

The northern Hecho basin overthrusts the central growth folds domain via the 100 km long Oturia fault. This major structure accommodates approximatively 5 km of shortening related to the emplacement of the Gavarnie thrust-sheet during Priabonian and early Rupelian (Labaume et al., 2016).

In the footwall of the thrust, the growth folds are related to the propagation of a shallower detachment in the 1500 m-thick, middle to late Eocene marls (Teixell, 1996). Magnetostratigraphic dating of the associated conglomerates deposits indicates a Priabonian – early Rupelian age for the successive folding events (Hogan, 1993; Hogan and Burbank, 1996; Labaume and Teixell, 2018). Recent magnetostratigraphic dating of the Orosia conglomerates in the eastern Jaca basin indicates that the Yebra anticline developed earlier during the Bartonian (Vinyoles et al., 2021). In contrast, dating of San Juan conglomerates in the central part of the basin suggests that both Atarès and Botaya anticlines (Fig. 1B) developed until the Aquitanian at least (Roigé et al.,

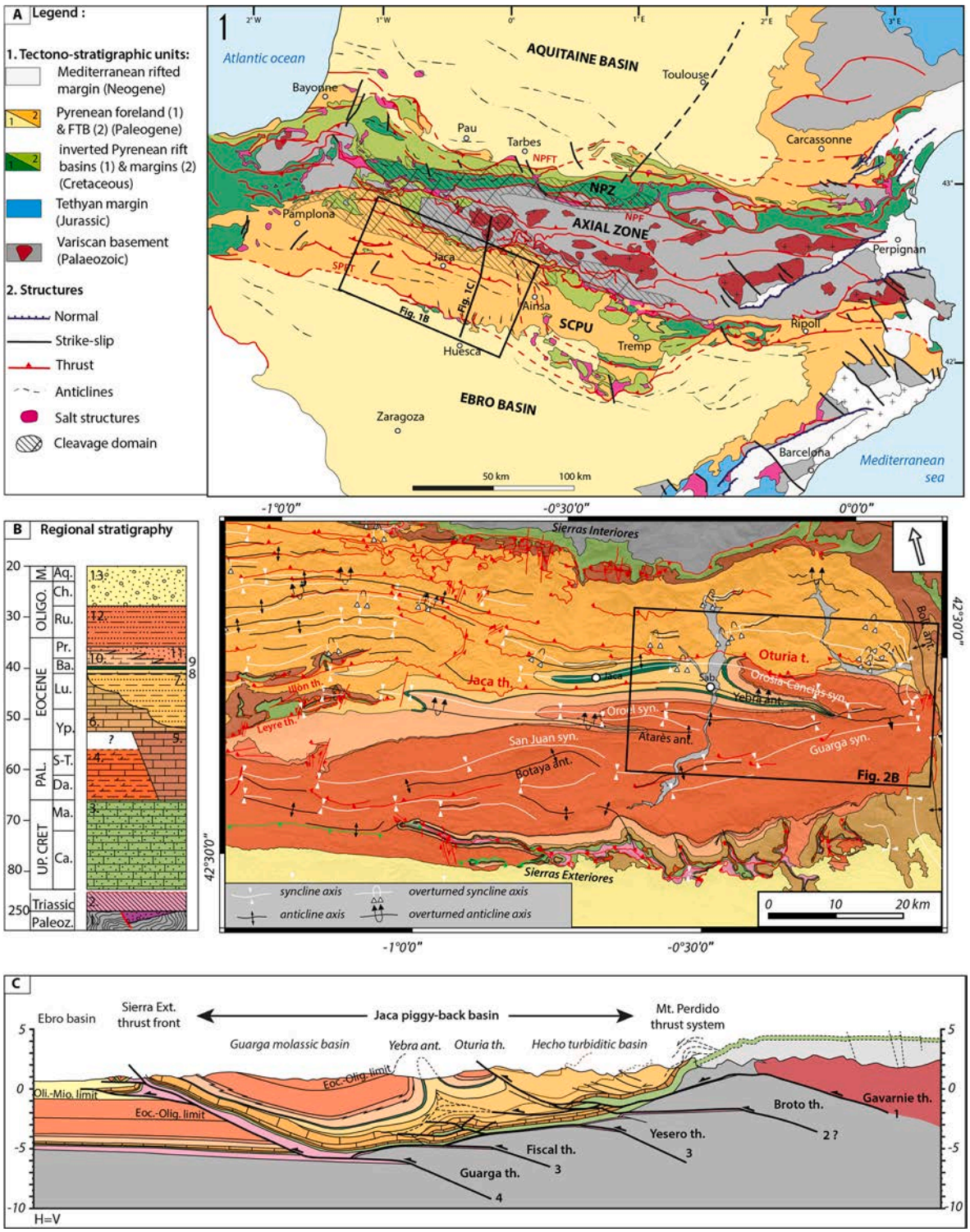

Fig. 1. A) Tectonic map of the Pyrenean belt, showing the main structural units and the area of cleavage in rocks. The black box refers to the Jaca basin. B) Regional stratigraphic column and synthetic geological map of the Jaca basin, modified from Labaume and Teixell (2018). The black box corresponds to the study area. (1: Variscan basement; 2: Keuper evaporites; 3: Marboré Sandstones; 4: Tremp formation; 5: Alveolina Limestones; 6: Boltaña and Guara Limestones; 7: Hecho Turbidites; 8: Fiscal-Larrès Marls; 9: Sabiñanigo Sandstones; 10: Pamplona Marls; 11 Belsué-Atarès Sandstones; 12: Campodarbe Group; 13: Uncastillo Formation). C) Geological cross-section of the eastern Jaca basin (modified from (Labaume et al., 2016). The section is located in the Fig. 1A).

2017).

To the south, the Guarga synclinorium developed in response to the uplift of the Sierras Exteriores at the southern margin of the basin. This complex tectonic area is characterized by the superimposition of N–S folds and E-W thrusts and folds involving the 50 m-thick, Upper Triassic evaporites which form the sole decollement level (Millan Garrido et al., 1994, 2000, 2006). The N–S folds are dated from growth strata to Bartonian - early Priabonian times and thus are related to the late stage of the Eaux-Chaudes thrusting and the onset of the Gavarnie thrusting (Labaume et al., 2016). Paleomagnetic data show that they developed

initially as NW-SE trending folds then undergone a 40° clockwise rotation in response to the emplacement of the South-Central Pyrenean thrust-sheets to the east (Pueyo, 2002; Mochales et al., 2012; Muñoz et al., 2013). The E-W thrusts and folds (referred hereafter as the Sierras Exteriores thrust front) are dated to late Rupelian and Aquitanian times from magnetostratigraphic dating of syn-tectonic alluvial fans deposited in the northern margin of the Ebro foreland basin (Hogan and Burbank, 1996; Millan Garrido et al., 2000; Oliva-Urcia et al., 2015, 2019).

2.2. Stratigraphy and tectono-sedimentary evolution of the jaca basin

The basement of the Jaca basin is composed of Palaeozoic sedimentary formations that were deformed and locally intruded by late Carboniferous granitoids during the Hercynian orogeny (Barnolas and Chiron, 1996). The dismantling of the Hercynian belt during the Permian-early Triassic period resulted in the deposition of alluvial red beds in continental rift basins (Lago et al., 2004; Lloret et al., 2021; Rodríguez-Méndez et al., 2014, 2016). During Middle and Upper Triassic were respectively deposited the Muschelkalk carbonates and Keuper evaporites in the whole Pyrenean domain. During the Upper Cretaceous, the Axial Zone of the Pyrenean belt and the northern edge of the Jaca basin was corresponding to the Iberian southern margin of an E-W trending rift system (Caldera et al., 2023). A thick platform carbonates succession (the Calcaires des Canyones formation) was deposited upon the previously eroded Palaeozoic - early Triassic basement (Fig. 1B). This carbonated platform progressively migrated southward from Cenomanian to Santonian times (Andrieu et al., 2021).

The foreland basin sequence started with the deposition of the Marboré Sandstones in a mixed carbonates-siliciclastic platform during the late Cretaceous (Garcés et al., 2020; Puigdefabregas and Souquet, 1986). These shallow-marine conditions persisted during the Palaeocene and the early Eocene in the northern part of the basin as it is attested by the deposition of the Alveolina Limestones formation (Fig. 1B). In contrast, fluvio-lacustrine deposits of the Tremp Fm that outcrop in the Sierra de Leyre and in the Sierras Exteriores, respectively in the central part and at the southern margin of the Jaca basin, record here the transition toward a continental environment (Nichols, 1987; Puigdefábregas, 1975).

During the lower-middle Eocene (56.0 - 41.2 Ma), the increasing flexural subsidence is marked by the deposition of the 4 km-thick deep-marine turbidites in the northern Hecho sub-basin (Labaume et al., 1985; Remacha and Fernández, 2003). The siliciclastic material, derived from eroding Pyrenean reliefs to the east, was delivered to the basin via axial routing systems (Caja et al., 2010; Gupta and Pickering, 2008). The Hecho turbidites onlap southward the ypresian Boltaña Limestones and the lutetian Guara Limestones formations that was both deposited in a shallow-marine platform upon the southward migrating forebulge (Mochales et al., 2012; Montes Santiago, 2009; Rodríguez-Pintó et al., 2012). Episodically, the tectonic destabilisation of carbonate platforms fed the foredeep depocenter in intrabasinal, coarse-grained materials that was resedimented as 200 m-thick beds of carbonated megabreccias (Barnolas and Teixell, 1994; Labaume et al., 1983, 1987; Payros et al., 1999). From the late Lutetian, the vertical axis clockwise rotation of the Boltaña anticline from a N100° axis to its actual N180° axis at the eastern edge of the Jaca basin (Mochales et al., 2012, 2016; Muñoz et al., 2013) is coeval with a change in the sediment routing system. At this time, the lower Bartonian Jaca turbidites system recorded the first north-derived input of clastic materials in the central Jaca basin (Caja et al., 2010; Gupta and Pickering, 2008; Oms et al., 2003; Remacha et al., 1995, 1998; Roigé et al., 2016).

During the Bartonian (41.2 – 37.8 Ma), the basin depocenter shifted southward and accommodated the deposition of more than 2000 m of shallow-marine marls and deltaic sandstones (Teixell, 1996). In the eastern Jaca basin, the lower 700 to 1000 m-thick Larrés-Fiscal Marls formation corresponds to blue-grey calcareous shales with slumps horizons and some interbeded sandstones/siltstones beds deposited in the external slope setting of carbonated ramps. They are overlapped by the 200 m thick Sabiñanigo Sandstones formation, that corresponds to deltaic sandstones beds alternating with fine-grained mudstones intervals. The Sabiñanigo sandstones allows the stratigraphic distinction between the underlying Larrès-Fiscal Marls and the overlying Pamplona Marls formation. This corresponds to blue-grey calcareous shales with some intercalated shelfal carbonates horizons. The thickness of the Pamplona marls is highly variable, from 100 m in the eastern part of the Yebra anticline to more than 2000 m in the central part of the Jaca basin. The Pamplona Marls are overlain by the westward prograding, 500 m-thick Atarès sandstones formation that records the progressive filling of the basin from east to west during the late Bartonian and Priabonian.

During the Priabonian (37.8–33.9 Ma) and the Rupelian (33.9–28.1 Ma), the deposition of the 3500 m-thick Campodarbe Group continental deposits in the Guarga depocenter marked the overfilling stage of the basin (Hogan, 1993; Hogan and Burbank, 1996; Puigdefábregas, 1975). These east-derived fluvial deposits are interdigitated with some local north-sourced alluvial conglomerates (the Bernuès Formation). These are, from east to west and older to younger, the late Eocene Santa Orosia-Cancias conglomerates, the late Eocene-early Oligocene Oroel conglomerates and the early Oligocene San Juan conglomerates (Roigé et al., 2017). From the latest Rupelian to the Aquitanian, the uplift of the Sierra Exteriores in response to the onset of the Fiscal and Guarga thrusting stoped the sedimentation in the basin (Oliva-Urcia et al., 2015, 2019). The main foreland depocenter was shifted southward in the actual Ebro foreland where Uncastillo Gp alluvial-fluvial sediments are deposited (Arenas and Pardo, 2001; Luzón, 2005).

2.3. The Oturia thrust fault and the Yebra anticline

This study focuses on the eastern part of the Jaca basin that is composed by the allochthonous Oturia thrust-sheet to the north and a N110°-trending growth folds pair to the south, corresponding to the Orosia-Cancias syncline and the Yebra anticline (Fig. 1B and 2). The Oturia thrust sheet is composed of late Ypresian-Lutetian Hecho turbidites, which are folded as a large hanging-wall ramp syncline with a general N110° trending axis (Labaume et al., 1985, 2016). To the east, the Hecho turbidites onlap the Boltaña Limestones formation and the folds curve in a N–S direction parallel to the Boltaña anticline axis (Mochales et al., 2016; Muñoz et al., 2013).

The Hecho turbidites overthrust southward the Bartonian-Priabonian shallow-marine to continental succession via the N110°-trending Oturia fault (Figs. 2B and 3). This 40° northward-dipping fault cuts the whole turbiditic succession and connects downward to an Upper Cretaceous hanging-wall ramp detached in the Upper Triassic (Fig. 1C). To the north, the Oturia fault connects to the Gavarnie basement thrust from which it accommodates approximatively 5 km of the total shortening (Labaume et al., 2016; Labaume and Teixell, 2018). The displacement rate along the Oturia thrust decreases eastward and the fault is replaced east of the Rio Ara valley by a fault-propagation anticline in the Hecho turbidites. Dating of thrust-involved units as well as syn-kinematic growth structures in the footwall indicate both a late Bartonian to Priabonian age for the main thrusting event (Labaume et al., 2016; Montes Santiago, 2009).

In the footwall of the Oturia fault, the Orosia-Cancias syncline (Figs. 2 and 3B) corresponds to a 30 km-long depocenter filled during folding with the Santa Orosia and the Laguarta-Cancias conglomerates units (Montes Santiago, 2009). In the northern limb, the Larrès Marls and the Sabiñanigo Sandstones lie in a reverse polarity with strata dipping from 70° to 35° northward. In contrast, the overlying Pamplona marls and Atarès Sandstones are thinning northward and strata dip with a normal polarity from 40° to 30° toward the south (Fig. 3B and D). These structural features show that the northern part of the Orosia-Cancias syncline developed in part in response to the uplift of the Oturia thrust-sheet to the north during Bartonian times (Labaume et al., 2016; Montes Santiago, 2009). To the south, the deltaic to alluvial

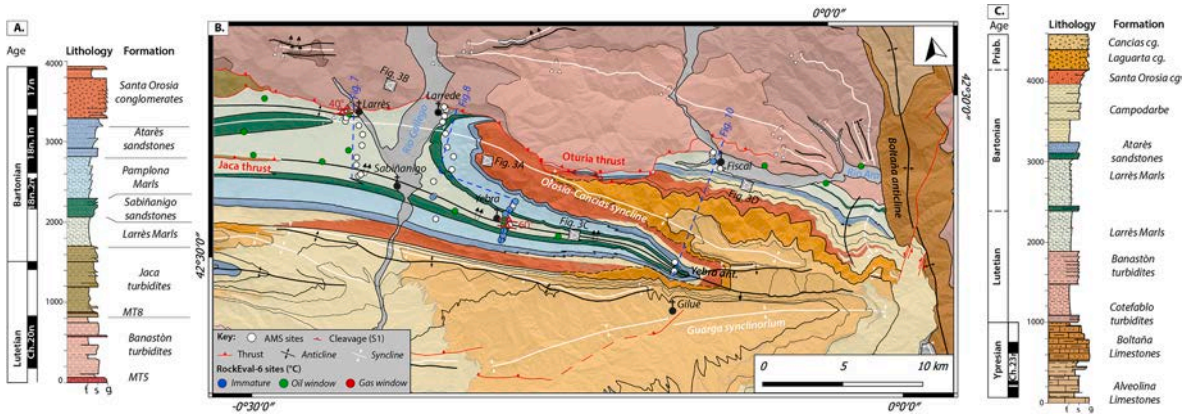

Fig. 2. A) Composite stratigraphic column of the western part of the study area in the Rio Aragon and Rio Gallego valley (modified from Oms et al., 2003; Roigé et al., 2016). B) Geological map of the study area (modified from Montes Santiago, 2009) Whites circles correspond to sampled sites for AMS analysis C) Synthetic stratigraphic column of the eastern part of the study area in the Rio Ara valley.

succession forms a stratigraphic wedge in the northern backlimb of the Yebra anticline, showing that both folds developed synchronously (Fig. 1C).

The Yebra anticline extends over 40 km from the Boltaña anticline at the eastern edge of the Jaca basin westward, where it is replaced by the 50 km-long Jaca thrust fault (Labaume and Teixell, 2018). This anticline is easily distinguishable in the basin landscape thanks to the Sabiñanigo Sandstones beds that highlight a south-verging overturned geometry (Fig. 3A and C). The fold limbs are both steeply dipping with an opposite polarity and stand in a physical contact in the hinge zone, which corresponds to highly strained marls of the Fiscal-Larrès unit (Larrasoaña et al., 1997). The Yebra anticline was interpreted as a detachment fold related to the buckling of the weak marly lithologies within the hinge zone (Larrasoaña et al., 1997; Millan Garrido et al., 2006; Teixell, 1996), in response to the propagation of a multi-detachment thrust system that connects to the Gavarnie basement thrust downward (Fig. 1C; Labaume et al., 2016; Labaume and Teixell, 2018). In the northern backlimb, the bedding presents a normal polarity with strata dipping northward from 50° in the Sabiñanigo sandstones to 20° in the Santa Orosia conglomerates (Fig. 3C). In the southern overturned forelimb, the deltaic units are dipping approximatively 80°–90° northward with a reverse polarity, whereas overlying conglomerates, that form the northern limb of the Guara synclinorium, are subvertical to 20° dipping southward.

These structural relationships attest that the main folding event of the Yebra anticline occurred during the late Bartonian-Priabonian synchronously with the deltaic and alluvial sedimentation. Syn-sedimentary growth geometries within these deposits allowed to reconstruct the folding kinematics. The progressive unconformity formed by the the Atarès and Santa Orosia formations evidences the early growth of the Yebra anticline during late Bartonian (Montes Santiago, 2009; Oms and Remacha Grau, 1992). Furthermore, the clast composition of the Santa Orosia conglomerates, dominated by sandstones remobilized from the northern Hecho turbidites, argues for the coeval uplift and exhumation of the Oturia thrust-sheet at this time (Roigé et al., 2016). Close to the Gilué town, at the eastern end of the Yebra anticline, the early Priabonian Laguarta conglomerates lie with an angular unconformity upon the sub-vertical late Bartonian Orosia Conglomerates (Montes and Colombo, 1996; Montes Santiago, 2009). This shows that the hinge of the Yebra anticline formed an eroding topographic high during the latest Bartonian - early Priabonian transition, and that the late Bartonian Santa Orosia conglomerates was uplifted at this time. Furthermore, the deposition of the Cancias conglomerates both in the Orosia-Cancias syncline and in the northern part of the Guarga synclinorium attests that the Yebra anticline was buried during the late Priabonian (Fig. 3C). Syn-sedimentary geometries and growth strata within these sequences in both limbs of the Yebra anticline attest that the fold continued to grow at this time (Montes Santiago, 2009). To the north, the erosion has removed the Laguarta and Cancias conglomerates in the footwall of the Oturia thrust, making it impossible to prove a tectonic activity of the fault at this time. However, the net enrichment in extrabasinal carbonated clasts sourced from northern Mesozoic units suggests an accelerated exhumation and erosion of the Oturia thrust-sheet at this time (Roigé et al., 2016, 2017).

3. Material and methods

3.1. Evolution of magnetic fabrics and AMS parameters in response to increasing strain in fold-and-thrust belts

The Anisotropy of Magnetic Susceptibility (AMS) is a standard method used to investigate the matrix strain record in various tectonic setting (Aubourg et al., 1995; Borradaile and Henry, 1997; Borradaile and Tarling, 1981; Borradaile and Jackson, 2004; Hrouda, 1982; Rochette et al., 1992; Tarling and Hrouda, 1993). The anisotropy of magnetic susceptibility in rocks is represented by a magnetic ellipsoid defined by the orientation of the three main susceptibility axis Kmax ≥ Kint ≥ Kmin. (Fig. 4). The Kmin axis corresponds to the pole of the magnetic foliation defined as the Kmax-Kint plane, whereas the Kmax reflects the magnetic lineation. In the case where the magnetic signal is carried by the crystallographic assemblage, such as clays, it allows to quickly assess the shape of the magnetic fabric which in turn reflect the matrix organisation. It is particularly powerful in weakly deformed rocks and mudrocks for which meso-scales structures are poorly developed or absent (Aubourg et al., 1995, 1999; Borradaile and Tarling, 1981; Kissel et al., 1986; Parés, 2004).

During the last decades, a lot of studies applied this technique in foreland fold and thrust belt settings to characterize the evolution of magnetic fabric during regional shortening (Averbuch et al., 1992; Boiron et al., 2020; Branellec et al., 2015; Lartigau et al., 2023; Parés et al., 1999). These studies showed that the evolution of the magnetic fabric can be considered as a good proxy of the early deformation of the rocks matrix related to the LPS stage that occurs prior to macro-scale faulting and folding (Averbuch et al., 1992; Parés et al., 1999). These works documented several types of magnetic fabrics evolving as successive stages of the cleavage development related to increasing strain (Fig. 4A). Immediately after deposition, rocks acquire an initial, type I, magnetic fabric, so called the sedimentary fabric, due to compaction and early diagenetic processes (Pueyo Anchuela et al., 2011). This fabric is characterized by well clustered Kmin axis around the pole-to-bedding, indicating thus a bedding-parallel magnetic foliation. In contrast, the Kmax axis are highly dispersed, without a clear definition of the magnetic lineation (Fig. 4A). The development of fractures network in rocks

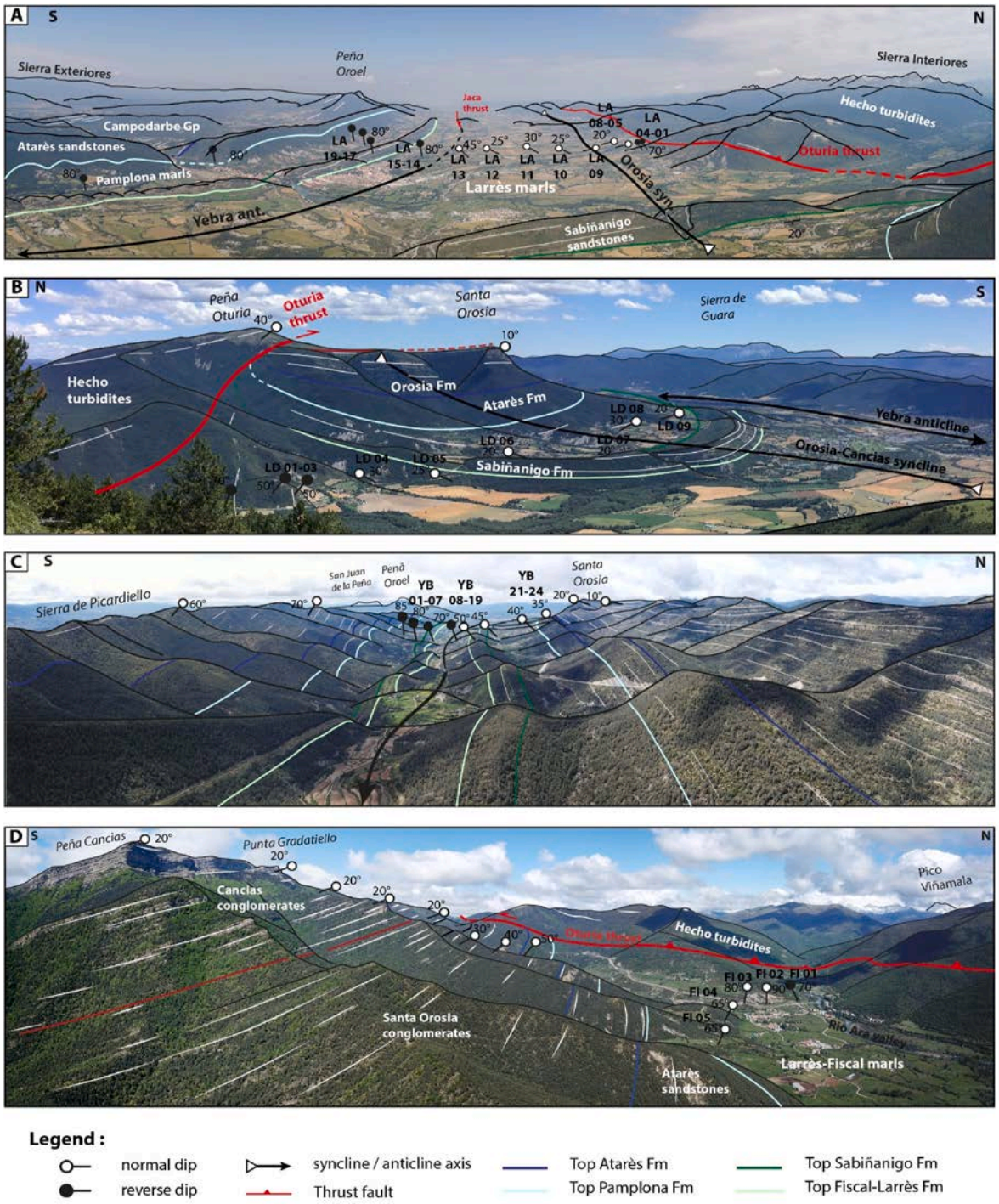

Fig. 3. Panoramic views of the Oturia thrust-sheet and the Orosia-Yebra growth folds pairs in the eastern Jaca basin. A) View of the western section, where Hecho turbidites are thrusting southward on the Larrès Marls via the Oturia fault. B) View of the central Larrede sub-section where Hecho turbidites are thrusting southward on the Santa Orosia conglomerates via the Oturia fault. C) View of the central Yebra sub-section showing the tighten hinge of the Yebra anticline. D) View of the eastern Fiscal section.

during the LPS stage is coeval with the development of an intermediate fabric. Type II fabrics are characterized by bedding-parallel Kmax axis that are progressively clustered perpendicular to the regional shortening, reflecting the apparition of a magnetic lineation (Fig. 4A), whereas Kmin axis are still clustered normal to the bedding. The increasing strain led to the development of cm-scale pencil structures as well as the loss of the magnetic foliation within rocks. The corresponding type III fabric exhibits a girdle distribution of the Kmin axis that reflect a poorly expressed magnetic foliation. In contrast, type IV fabrics are characterized by clustering Kmin axis parallel to the bedding that record the rejuvenation of a perpendicular, tectonic controlled magnetic foliation. This is accompanied by the development of a cleavage in rocks. Finally, the development of a slaty cleavage within rocks is accompanied by the apparition of the type V fabric. This is characterized by the spreading of the Kmax axis along a plane normal to the Kmin axis and reflect a tectonic-controlled foliation. This scheme was popularised in the review article by Parés (2015).

The characterization of magnetics fabrics was historically based on

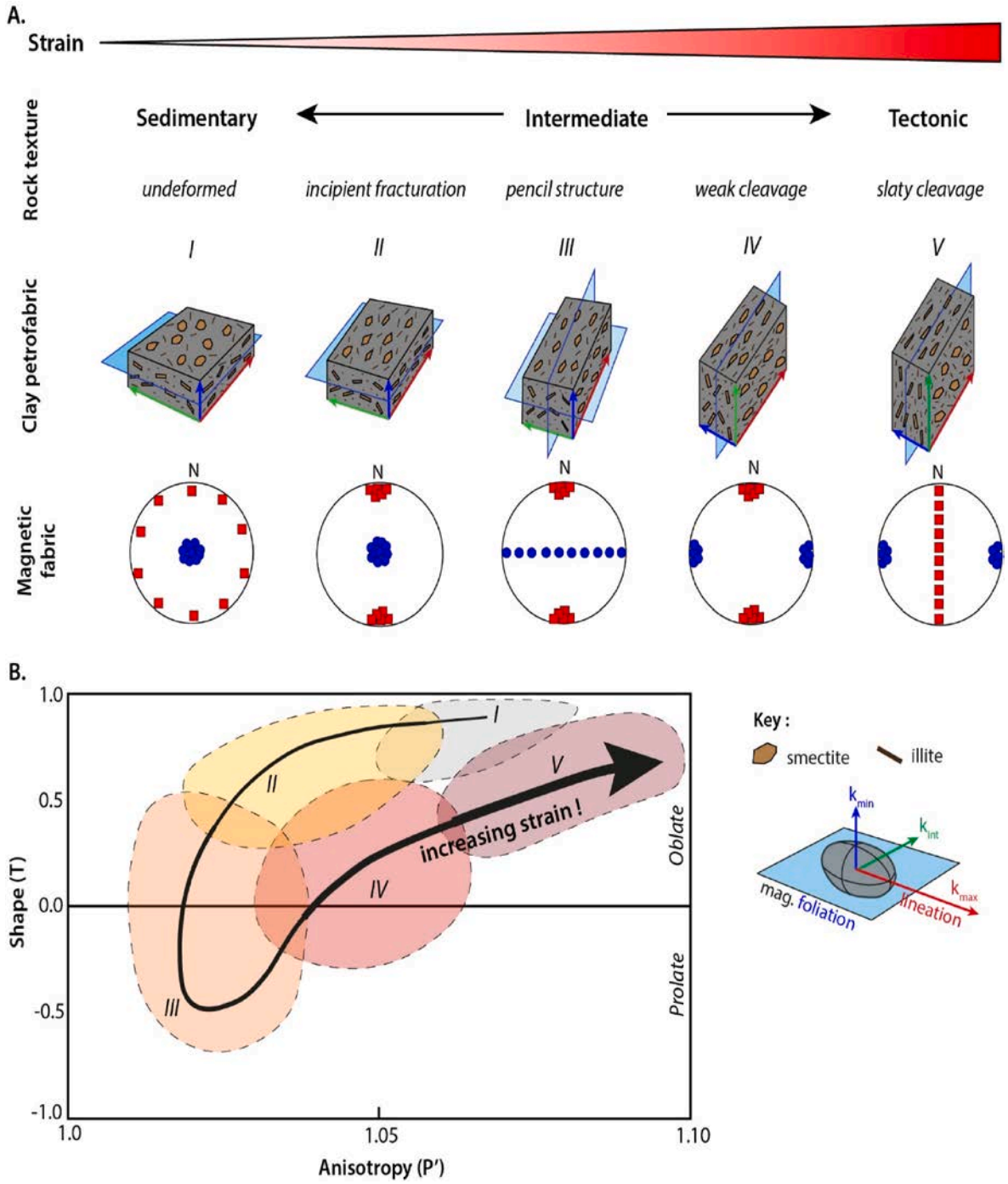

Fig. 4. A) The basic principle of AMS in weakly deformed rocks, showing the five-stage evolution of magnetic fabrics with the increasing strain B) Pathway of the coeval evolution of T-P′ anisotropy parameters represented in a Jelinek's diagram.

the orientation and distribution of the main susceptibility axis from the analysis of oriented rock fragments. In the Pyrenean belt, AMS studies have all demonstrated that Kmin axis was oriented normal to the regional bedding within undeformed or poorly strained rocks, then was progressively reoriented normal to the cleavage plane (S1) during increasing strain (Pocoví Juan et al., 2014). In contrast, the magnetic lineation in the cleavage domain is oriented N110° parallel to the mains structures and in a right angle with the Pyrenean shortening direction (Larrasoaña et al., 1997; Pueyo Anchuela et al., 2010, 2012a, 2012b). As a consequence, these observations allow to be predictable concerning the orientation of the main susceptibility axis in area where the regional tectonic context is clearly documented, such as the west-central Pyrenees (Pocoví Juan et al., 2014).

In parallel, some studies demonstrated that the anisotropy parameters, corresponding to the corrected degree of anisotropy (P′) and the shape parameters (T), show a progressive evolution in response to the increasing strain within rocks (Boiron et al., 2020; Gracia-Puzo et al., 2021; Parés, 2004). The degree of anisotropy (P) is defined as the ratio of the magnetic lineation (L) versus the magnetic foliation (F), where the magnetic foliation corresponds to Kint/Kmin and the magnetic lineation corresponds to Kmax/Kint. As such, the degree of anisotropy is equivalent to the ratio between the Kmax and the Kmin main susceptibility. The degree of anisotropy is usually corrected of the shape of the

magnetic ellipsoid following the equation: $P' = P^a$, where $a = \sqrt{\left(1 + \frac{T^2}{3}\right)}$. The shape parameter (T) is calculated from the main susceptibilities following the relation: $T = \frac{ln\left(\frac{Kint}{Kmin}\right) - ln\left(\frac{Kmax}{Kint}\right)}{ln\left(\frac{Kint}{Kmin}\right) + ln\left(\frac{Kmax}{Kint}\right)}$. The value of the T parameter ranges between −1 and 1. When the T values is negative, the corresponding magnetic fabric is prolate and displays a cigar-like shape. In contrast, a positive T parameter indicates an oblate magnetic fabric that is characterized by a disc-like shape.

The corelated evolution of both parameters during the matrix strain is classically represented as a characteristic loop-like T-P′ path in a Jelinek's diagram (Fig. 4B) (Gracia-Puzo et al., 2021; Jelínek, 1978; Parés, 2004). The type I sedimentary fabrics are characterized by an oblate magnetic fabric that reflects the bedding-controlled magnetic foliation. They are characterized by high values of the shape parameter as well as the degree of anisotropy, respectively close to 1 and 1.10 (Aubourg et al., 2004; Gracia-Puzo et al., 2021; Parés, 2004). The development of type II fabric during early deformation stages is associated with a coeval decrease of the degree of anisotropy and the shape parameter that reflects the transition toward weakly oblate or triaxial magnetic fabric. In the Arro-Fiscal Marls that lie in the western Jaca basin, type II fabrics are characterized by P′ parameters ranging between 1.05 and 1.09 and T parameters between 0.4 and 1 (Boiron et al., 2020; Gracia-Puzo et al., 2021). The loss of magnetic foliation in type III fabrics is coeval with the apparition of a prolate magnetic shape characterized by a very low degree of anisotropy and negative value of the T parameter. In the Arro-Fiscal Marls of the western Jaca basin, this step is defined with P′ values comprised between 1.03 and 1.06 and T values between −0.4 and 0.4 (Boiron et al., 2020; Gracia-Puzo et al., 2021). For increasing strain, the development of a tectonic-controlled magnetic foliation in type IV and type V fabrics is recorded by the rejuvenation of the oblate magnetic fabric. In the Arro-Fiscal Marls of the western Jaca basin, type IV fabric are characterized by increasing P′ values form 1.05 to 1.1 associated with T values between 0 and 0.5 (Boiron et al., 2020; Gracia-Puzo et al., 2021). Type V fabrics are characterized by P′ value close to 1.10 associated with T values comprised between 0.5 and 1.0 (Boiron et al., 2020; Gracia-Puzo et al., 2021).

Recent works have shown that the analysis of anisotropy parameters is as predictable as the characterization of main susceptibly axis in oriented samples to assess the matrix strain degree related to shortening (Boiron et al., 2020; Gracia-Puzo et al., 2021). Furthermore, this method presents two non-negligible advantages. The first is that the evolution of P' and T values is more progressive than the orientation changes of the main susceptibilities axes during strain (Boiron et al., 2020). Secondly, this method can be applied to non-oriented samples, which facilitates sampling and speeds up the analysis of ASM in the laboratory, especially for weakly consolidated mudrocks (Gracia-Puzo et al., 2021). In this study, we chose thus to characterize the magnetic fabrics in the Larrès and Pamplona marls by analysing the anisotropy parameters P and T within.

3.2. Sampling and AMS analysis

In order to assess the effect of thrusting, folding and syn-tectonic sedimentation on the matrix strain within the Larrès and Pamplona Marls, we sampled four sub-parallel sections in the eastern Jaca basin that trends perpendicular to the Oturia fault and the Yebra anticline. The Larrès section (Fig. 3A) is located in the western part of the study area, where no evidence of syntectonic conglomerates deposition could be evidenced in the Orosia-Cancias depositional syncline. The Larrede and Yebra sections (Fig. 3B and C) in the central part of the study area are located respectively beneath and forward of the Bartonian Santa Orosia conglomerates, in a location corresponding approximatively to the former apex of the Santa Orosia alluvial fan. Three additional sites were sampled in the southern part of the Larrede section to enable a correlation with the Yebra section. Both sections are presented in the following as a one single composite section. The Fiscal section is located in the eastern part of the study area and is divided in two segments in either side of the Peña Cancias massif. The northern transect (Fig. 3D) was sampled near the Fiscal town within marls lying beneath the conglomerate units in the footwall of the Oturia fault, in a similar setting than the Larrede section. The southern segment is composed by three sites lying forward of the conglomerates at the eastern pericline hinge of the Yebra fold (Fig. 2B).

Along each section, sites were sampled and numerated from the outcropping Oturia fault plane southward. Sites were regularly spaced following a 200–300 m step, which were reduced to 50–80 m in the neighbouring of the Oturia fault and within the hinge of the Yebra anticline. Unoriented samples was collected from fresh rocks at the outcrops, then cut into 1–3 g rock fragments at the laboratory. For each site, 15–20 unoriented fragments was thus analysed in order to obtain a statistically significant value of the anisotropy parameters P' and T, following the protocol described in (Gracia-Puzo et al., 2021).

The Anisotropy of low-field Magnetic Susceptibility (AMS) was measured with a MFK1-fa Kappabridge by using standard magnetic field strength (200 A/m) and frequency (976 Hz). The unoriented tensor of the magnetic susceptibility and the value of anisotropy parameters measured in each fragment were computed using the AGIGO software. In order to obtain an average value of the mean magnetic susceptibility and anisotropy parameters for each site, we applied the statistical method of Jelínek (1978).

In order to identify the mineral fraction and magnetic components that support the susceptibility signal within the studied marls formations, we carried out furthermore analysis of the mineralogical composition, rock magnetism and organic matter content of some selected samples along the four sections. The mineralogical composition of four Larrès marls and three Pamplona marls samples was characterized by X-ray diffraction analysis (UPPA, France). As the results were homogeneous whatever the sample location and stratigraphic unit, we then selected one Larrès marls (sample YB-16) and one Pamplona Marls (sample YB-04) for investigating magnetic hysteresis properties using a Vibrating Sample Magnetometer (IPMC-Sorbonne University, Paris, France). Finally, the organic matter content and maturity was characterized by a RockEval6 analysis (Sorbonne University, France) (Behar et al., 2001; Lafargue et al., 1998).

4. Results

4.1. Composition and rock magnetism of Larrès and Pamplona Marls

The Larrès and Pamplona Marls formations present both a homogeneous lithofacies corresponding to poorly consolidated blue-grey mudstones, with some intercalated dm-thick beds of sandstones (Montes Santiago, 2009; Puigdefábregas, 1975).

X-ray diffraction analysis has shown that the Larrès and Pamplona marls have a homogeneous mineralogical composition (Sup. Mat.), dominated by calcite minerals and quartz grains, with a small proportion of clay particles (illite, chlorite and smectite).

The RockEval 6 experiments indicates furthermore a very low content in organic matter (TOC <1%) both in the Larrès and Pamplona Marls in the whole study area. The measured Tmax values ranged from 421 °C to 438 °C (Fig. 2B), reflecting a low and homogeneous burial of both units that did not exceed the onset of the oil window in our study area.

As calcite and quartz are diamagnetic components, the mineralogical composition of the Larrès and Pamplona marls suggests that the AMS signal is supported by the clay fraction, which corresponds to a detrital smectite-illite assemblage. The hysteresis loop of Larrès Marls and Pamplona Marls (Sup. Mat.) display both a paramagnetic component. No hysteresis signal was observed, indicating that the ferromagnetic fraction is very low in these marls. Magnetic susceptibility is therefore largely controlled by the paramagnetic clay fraction.

4.2. Magnetic fabrics in the Larrès and Pamplona Marls

The mean magnetic susceptibility (Km) in the 978 analysed rock fragments varied between 80.10^{-6} and 250.10^{-6} SI and 90% of the measured values between 100.10^{-6} and 200.10^{-6} SI (Fig. 5A). This is comparable to what was reported for the Arro-Fiscal and Pamplona marls in the western Jaca basin (Boiron et al., 2020; Gracia-Puzo et al., 2021; Larrasoaña et al., 1997; Pocoví Juan et al., 2014; Pueyo Anchuela et al., 2011; Pueyo-Morer et al., 1997), and is consistent with a dominant paramagnetic contribution to the AMS signal.

The degree of anisotropy (P′) averaged per site (Fig. 5B) ranges between 1.02 and 1.08, that is globally lower than what was measured in the stratigraphically equivalent Arro-Fiscal Marls formation in the Siguës area (Boiron et al., 2020; Gracia-Puzo et al., 2021). This difference may be related to either a lower intrinsic anisotropy of the magnetic particles or a less tuned preferential orientation of the magnetic minerals in our study area. P′ values in the Pamplona Marls (Fig. 5B) are lower than those in the Larrès-Fiscal formation for the same susceptibility range. If we extend this comparison to the Arro-Fiscal Marls further west, which show a greater degree of burial (Boiron et al., 2020), it seems realistic to think that the P' value is more sensitive to the degree of compaction resulting from the sedimentary burial rather than to the expression of a different magnetic mineralogy. The average values of the shape parameter (T) ranges between −0.05 and 0.90 (Fig. 5C) with only two sites displaying a negative value characteristic of a prolate shape. This indicates that the Larrès and Pamplona marls in our study are dominated by an oblate magnetic ellipsoid, which corresponds to a well-developed magnetic foliation controlling a disc-shaped magnetic fabric.

Four characteristic types of magnetic fabric can be described in our study area, based on general trends of the P' vs. T values observed in both the Larrès and Pamplona Marls (Fig. 6).

In the diagram of the evolution of the magnetic fabric from type I to V (Fig. 4), only oriented samples make it possible to distinguish type I from type II, not scalar data such as P' and T. All studies of the magnetic fabric in the Eocene marls of the Jaca basin (Larrasoaña et al., 1997; Pocoví Juan et al., 2014; Pueyo Anchuela et al., 2011) have shown the ubiquity of magnetic lineations controlled by the N110° trending axis. We have therefore chosen to classify our least deformed fabric as type II. Note that this nomenclature differs from that used by Gracia-Puzo et al. (2021).

The type II is the most dominant magnetic fabric in our study, and was defined from 28 sites where 1.03 to 1.06 P' values are associated with 0.40–0.80 T values (Table 1). This type II records a flattened fabric controlled by magnetic foliation, as expressed by the relatively narrow 95% confidence ellipses around the Kmin axis, the E23 values that range between 5° and 20°. Type II marls are characterized by a poorly developed fractures network (Fig. 6B) that is a marker of an incipient deformation (Fig. 6D–H).

The type III magnetic fabric is characterized by eighteen sites that shares a very low value of the anisotropy P' ranging between 1.02 and 1.05, as well as the T parameter, with values ranging between −0.05 and 0.40 (Table 1). In type III fabric, the standard deviation of the T parameter is higher than other types, but the most striking feature is the enlargement of the 95% confidence ellipse of the Kmin axis, associated with high values of the E23 parameter which ranges from 10° to 50°. Together, these scalar parameters highlight an overall triaxial fabric that dominates in corresponding sites. This trend highlights an overall decrease in the expression of the magnetic foliation. In outcrops, type III marls are distinguishable through their stretched linear aspect (Fig. 6) that characterizes the development of elongated pencil structures (Fig. 6C–F).

The type IV magnetic fabric is defined by six sites with high P′ 1.05 to 1.07 and T between 0.00 and 0.50 values (Table 1). The T standard deviation is still significant although lower than in the case of type II fabric, but here the P' standard deviation is higher. The 95% confidence ellipse can be quite wide or quite narrow. E23 values range from 5° to 10°. These features highlight a weakly oblate magnetic fabric controlled by the superimposition of magnetic lineation and foliation. Marls of type IV magnetic fabric outcrop as semi-consolidated and highly fractured rocks in which can be distinguished some incipient, sub-parallel and cm-spaced cleavage planes (Fig. 6B–E).

Finally, the type V magnetic fabric is defined from ten sites that have the highest degree of anisotropy P′ and shape parameter T. P' ranges between 1.06 and 1.09 with a relatively high standard deviation. T is higher than 0.50 with a low standard deviation that is characteristic of a well-developed oblate fabric. It is consistent with the very tight 95% confidence ellipse of the Kmin axis and E23 parameter lower than 12°. Marls of type V correspond to more competent shales displaying mm-spaced S1 planes which are characteristic of a slaty cleavage (Fig. 6A–G).

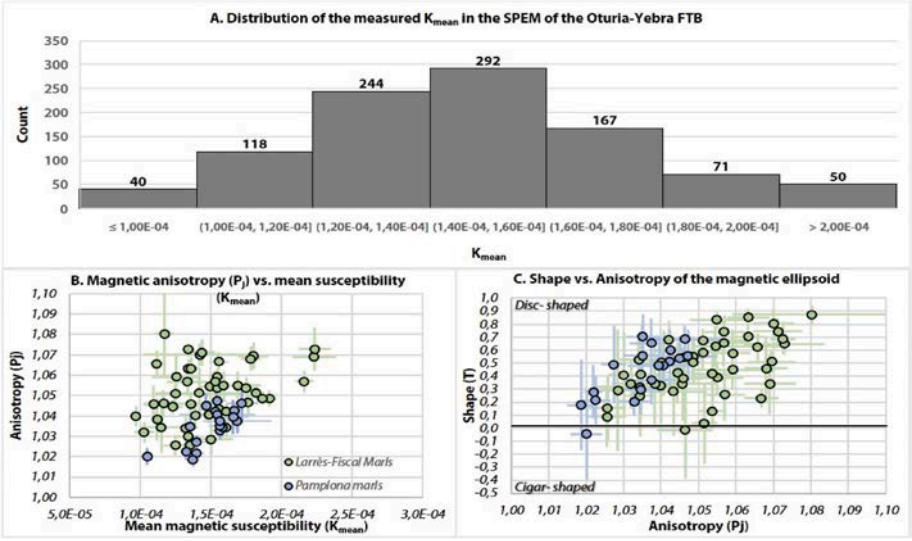

Fig. 5. A) Distribution of the measured mean magnetic susceptibility in all samples/B) Plot of site-average Anisotropy (P′) versus mean Magnetic susceptibility (Kmean). C) Jelinek T-P′ diagram of all analysed sites.

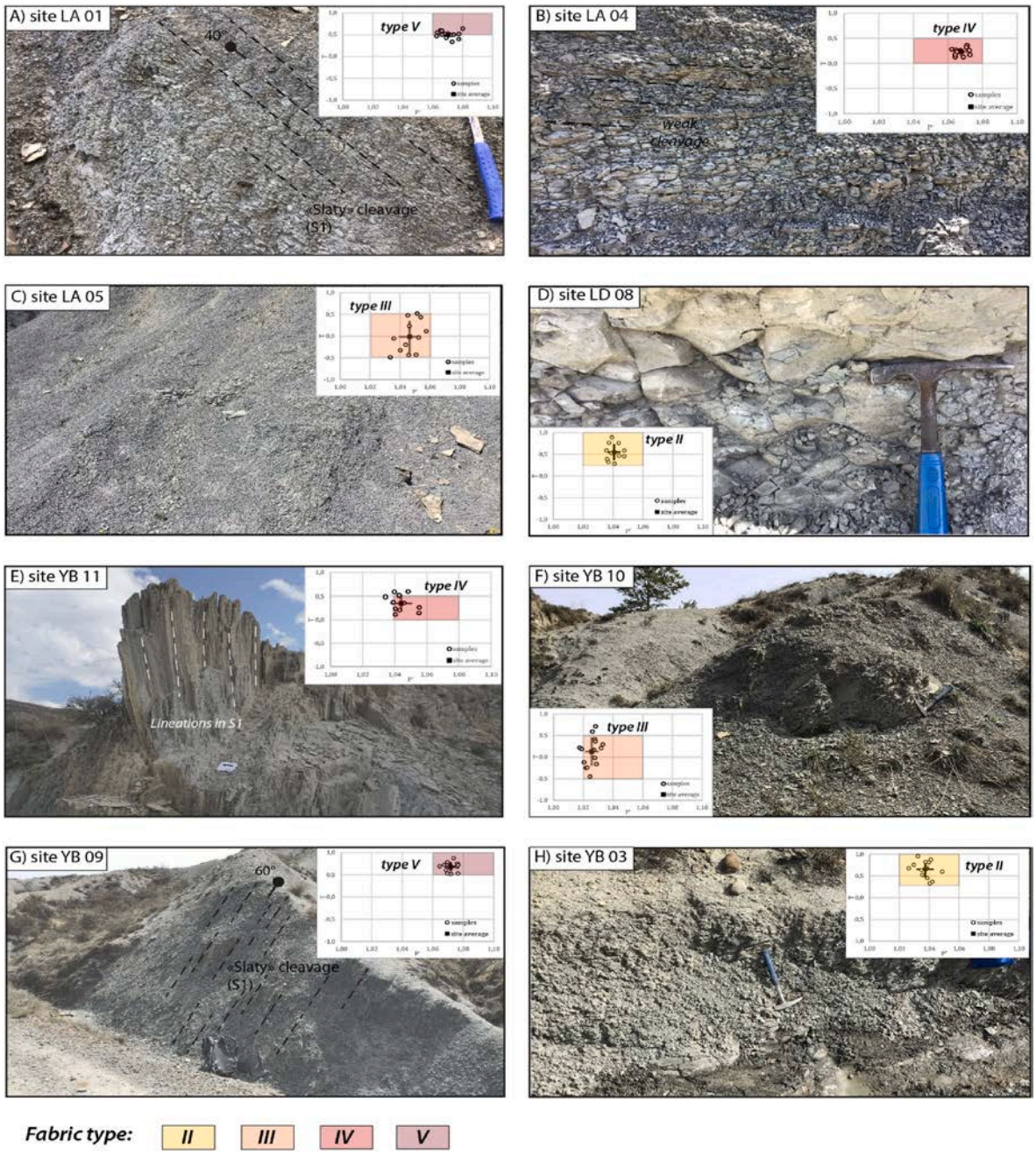

Fig. 6. Outcrop photographs of some sampled sites in different structural settings. A) slaty cleavage in the footwall of the Oturia thrust, Larrès section (<50 m from the fault). B) Development of a weak, cm-spaced cleavage planes, Larrès section (200 m from the fault). C) Strongly fractured marls, Larrès section (300 m from the fault). D) Undeformed to poorly deformed mudstones, Larrede section (1500 m from the fault). E) Lineation developed in cleavage planes within the hinge of the Yebra anticline, Yebra section. F) Strongly fractured mudstones, 100 m to the south of the site YB 11. G) Cleavage planes in mudstones within the fold hinge, Yebra section. H) Weakly deformed mudstones lying in the overturned forelimb of the Yebra anticlie, Yebra section.

4.3. Evolution of magnetic fabrics in the footwall of the Oturia thrust and across the Yebra anticline

4.3.1. The Larrès section

The Larrès section contains eighteen sites distributed over 5700 m in the footwall of the Oturia thrust toward the foreland (Fig. 7). Fifteen sites were sampled in the Larrès marls outcropping between the Oturia thrust and the hinge of the Yebra anticline and three sites were sampled in the Pamplona marls lying in the southern sub-vertical forelimb.

At the first order, the magnetic fabrics are dominantly oblate and controlled by the magnetic foliation although fives sites are characterized by a roughly triaxial to prolate shape with approximatively equivalent lineation vs. foliation parameters (Fig. 7A). Among the Larrès marls sites, the four different types of magnetic fabrics were recognized whereas the Pamplona marls record only a type III magnetic fabric (Fig. 7B).

In the footwall of the Oturia thrust, the Larrès marls are characterized first by a type V fabric, at the LA 01 site located <50 m in horizontal distance from the fault (Figs. 6F–. 7C and 7D–. E). Between 100 and 250 m, the following LA 02, LA 03 and LA 04 sites are characterized by a type IV magnetic fabric. Although anisotropy data overlap between the different types, it seems logical to assign type IV, which could also be compared to type II, as it follows type V, itself clearly identified in the field, with the development of a developed slaty cleavage.

Table 1
The location (site, long, lat), formation, bedding, measured samples (n), anisotropy parameters, standard deviation and fabric type of each analysed sites.

site	longitude	latitude	n	formation	bedding	d (m)	K_{mean}	σ_{kmean}	L	σL	F	σF	P'	$\sigma_{P'}$	T	σ_T	e23	σ_{e23}	Fabric
LA_01	−0,383,781	42,567,168	13	Larrès-Fiscal	N308°/60°	20	1,80E-04	1,09E-05	1016	0,003	1050	0,004	**1070**	0,006	**0,502**	0,084	**5069**	1545	Type V
LA_02	−0,383,985	42,566,183	14	Larrès-Fiscal	N132°/48°	100	2,16E-04	6,50E-06	1020	0,006	1035	0,006	**1057**	0,005	**0,257**	0,200	**6614**	2253	Type IV
LA_03	−0,384,275	42,565,192	13	Larrès-Fiscal	N115°/22°	180	2,23E-04	1,53E-05	1022	0,007	1045	0,009	**1069**	0,007	**0,342**	0,233	**4308**	1169	Type IV
LA_04	−0,384,886	42,564,204	13	Larrès-Fiscal	N117°/17°	250	1,78E-04	7,08E-06	1018	0,009	1047	0,005	**1068**	0,006	**0,458**	0,251	**5046**	1580	Type IV
LA_05	−0,387,712	42,563,916	12	Larrès-Fiscal	N320°/40°	280	1,76E-04	6,83E-06	1022	0,008	1023	0,010	**1046**	0,007	**−0,015**	0,371	**14,900**	8687	Type III
LA_06	−0,387,526	42,562,322	12	Larrès-Fiscal	N317°/13°	480	1,82E-04	5,69E-06	1024	0,008	1026	0,008	**1052**	0,003	**0,037**	0,313	**9042**	4041	Type III
LA_07	−0,388,984	42,561,240	14	Larrès-Fiscal	N117°/29°	590	1,69E-04	1,65E-05	1016	0,003	1037	0,006	**1055**	0,007	**0,389**	0,127	**6171**	2071	Type II
LA_08	−0,390,093	42,559,417	13	Larrès-Fiscal	N117°/21°	790	1,55E-04	6,70E-06	1025	0,003	1040	0,004	**1067**	0,005	**0,230**	0,075	**6433**	2294	Type IV
LA_09	−0,380,879	42,555,564	13	Larrès-Fiscal	/	1070	1,75E-04	8,22E-06	1015	0,004	1037	0,006	**1054**	0,005	**0,417**	0,161	**5446**	1773	Type II
LA_10	−0,379,376	42,550,170	14	Larrès-Fiscal	N316°/23°	1550	1,54E-04	3,91E-06	1012	0,005	1044	0,005	**1059**	0,005	**0,577**	0,181	**4250**	0,918	Type II
LA_11	−0,381,545	42,544,282	12	Larrès-Fiscal	N305°/30°	2220	1,36E-04	6,17E-06	1008	0,002	1047	0,007	**1060**	0,009	**0,703**	0,093	**3900**	0,839	Type II
LA_12	−0,387,356	42,538,236	14	Larrès-Fiscal	N280°/25°	3030	1,48E-04	1,04E-05	1010	0,005	1029	0,005	**1041**	0,004	**0,499**	0,251	**8264**	3630	Type II
LA_13	−0,388,770	42,534,205	13	Larrès-Fiscal	N320°/46°	3490	1,42E-04	3,98E-05	1006	0,004	1057	0,005	**1070**	0,005	**0,805**	0,111	**4085**	0,933	Type V
LA_14	−0,386,946	42,528,472	12	Larrès-Fiscal	/	4040	1,42E-04	3,12E-05	1008	0,003	1040	0,010	**1051**	0,012	**0,675**	0,090	**6683**	3068	Type V
LA_15	−0,388,805	42,527,869	14	Larrès-Fiscal	N292°/81°	4130	1,49E-04	7,15E-06	1009	0,004	1041	0,006	**1055**	0,006	**0,630**	0,160	**7086**	2371	Type V
LA_17	−0,393,575	42,521,559	13	Pamplona	N296°/81°	4940	1,05E-04	4,91E-06	1010	0,004	1009	0,004	**1020**	0,004	**−0,045**	0,347	**44,123**	23,369	Type III
LA_18	−0,400,128	42,519,722	13	Pamplona	/	5350	1,40E-04	5,94E-06	1008	0,003	1014	0,002	**1022**	0,002	**0,280**	0,205	**17,200**	4010	Type III
LA_19	−0,400,215	42,517,425	12	Pamplona	N285°/80°	5590	1,37E-04	5,14E-06	1008	0,004	1011	0,004	**1019**	0,004	**0,179**	0,350	**29,183**	13,307	Type III
LD_01	−0,314,469	42,555,948	10	Larrès-Fiscal	N280°/50°	150	2,23E-04	1,13E-05	1012	0,003	1056	0,008	**1073**	0,011	**0,649**	0,083	**3170**	1066	Type V
LD_02	−0,314,151	42,555,682	12	Larrès-Fiscal	N275°/55°	170	1,91E-04	5,29E-06	1010	0,004	1036	0,005	**1049**	0,004	**0,548**	0,158	**5555**	1410	Type V
LD_03	−0,313,500	42,554,231	13	Larrès-Fiscal	N292°/55°	280	1,55E-04	4,65E-06	1023	0,004	1030	0,004	**1054**	0,004	**0,132**	0,137	**6608**	1948	Type IV
LD_04	−0,315,696	42,550,911	14	Larrès-Fiscal	N080°/20°	690	1,56E-04	1,49E-05	1014	0,006	1027	0,010	**1043**	0,009	**0,281**	0,338	**9536**	6597	Type III
LD_05	−0,317,971	42,547,895	14	Larrès-Fiscal	N080°/30°	1075	1,61E-04	6,69E-06	1012	0,004	1021	0,006	**1034**	0,005	**0,248**	0,273	**11,757**	4913	Type III
LD_06	−0,317,650	42,541,177	10	Pamplona	N060°/20°	1620	1,56E-04	5,01E-06	1013	0,003	1019	0,002	**1033**	0,004	**0,205**	0,109	**11,690**	4789	Type III
LD_07	−0,318,623	42,533,478	13	Pamplona	N350°/15°	2400	1,58E-04	4,91E-06	1012	0,003	1022	0,004	**1034**	0,004	**0,298**	0,188	**12,015**	4401	Type III
LD_08	−0,315,283	42,527,590	15	Pamplona	N005°/15°	2800	1,53E-04	6,45E-06	1010	0,005	1030	0,004	**1042**	0,005	**0,515**	0,196	**9607**	2772	Type II
LD_09	−0,318,529	42,520,745	15	Pamplona	N330°/22°	3630	1,46E-04	4,48E-06	1010	0,004	1033	0,006	**1045**	0,006	**0,540**	0,162	**9733**	2754	Type II
LD_10	−0,333,962	42,516,322	13	Larrès-Fiscal	N303°/33°	4700	1,35E-04	5,43E-06	1010	0,005	1024	0,007	**1035**	0,006	**0,411**	0,324	**14,885**	6567	Type II
LD_11	−0,335,999	42,508,263	11	Larrès-Fiscal	/	5550	1,59E-04	1,28E-05	1004	0,001	1045	0,006	**1055**	0,007	**0,833**	0,062	**5245**	1594	Type V
LD_12	−0,338,146	42,495,492	11	Pamplona	N2898°/77°	6850	1,32E-04	3,34E-06	1009	0,003	1013	0,003	**1023**	0,004	**0,215**	0,187	**15,745**	5336	Type III
YB_01	−0,292,980	42,476,300	14	Pamplona	N285°/75°	5795	1,56E-04	8,03E-06	1005	0,003	1027	0,004	**1035**	0,005	**0,704**	0,170	**14,571**	4213	Type II
YB_02	−0,292,492	42,476,652	12	Pamplona	N284°/81°	5720	1,40E-04	8,44E-06	1006	0,004	1019	0,005	**1027**	0,003	**0,490**	0,296	**23,792**	13,432	Type II
YB_03	−0,291,580	42,476,989	13	Pamplona	N293°/80°	5650	1,68E-04	2,45E-05	1006	0,004	1028	0,004	**1037**	0,006	**0,652**	0,194	**15,662**	4177	Type II
YB_04	−0,291,208	42,478,184	14	Pamplona	N309°/71°	5520	1,72E-04	1,12E-05	1007	0,003	1036	0,008	**1046**	0,010	**0,683**	0,105	**13,207**	4755	Type II
YB_05	−0,290,562	42,478,880	14	Sabiñanigo	N290°/68°	5420	1,35E-04	5,16E-06	1007	0,004	1026	0,005	**1035**	0,005	**0,556**	0,242	**20,136**	6142	Type II
YB_06	−0,289,437	42,480,341	10	Sabiñanigo	N290°/80°	5240	1,32E-04	2,95E-06	1008	0,004	1024	0,004	**1034**	0,005	**0,527**	0,198	**18,320**	4273	Type II
YB_07	−0,289,385	42,481,146	13	Sabiñanigo	N285°/73°	5160	1,34E-04	8,95E-06	1008	0,005	1020	0,005	**1030**	0,004	**0,409**	0,322	**26,454**	16,416	Type II
YB_10.5	−0,288,569	42,483,641	12	Larrès-Fiscal	N284°/57°	4900	1,16E-04	1,39E-05	1010	0,004	1034	0,004	**1046**	0,007	**0,544**	0,129	**17,925**	3853	Type IV
YB_08	−0,286,354	42,482,971	14	Larrès-Fiscal	N290°/61°	4870	1,25E-04	1,73E-05	1015	0,005	1041	0,009	**1059**	0,011	**0,449**	0,151	**19,750**	9677	Type IV
YB_11.5	−0,288,403	42,484,050	13	Larrès-Fiscal	N297°/65°	4850	1,03E-04	6,81E-06	1010	0,003	1021	0,005	**1032**	0,005	**0,340**	0,189	**26,946**	9348	Type III
YB_09	−0,285,843	42,483,455	12	Larrès-Fiscal	N294°/62°	4800	1,34E-04	4,99E-06	1010	0,004	1056	0,004	**1072**	0,003	**0,685**	0,110	**6658**	1248	Type V
YB_12.5	−0,287,725	42,484,766	13	Larrès-Fiscal	N291°/48°	4760	1,23E-04	6,56E-06	1012	0,005	1030	0,005	**1044**	0,004	**0,427**	0,234	**14,592**	4123	Type IV
YB_10	−0,285,128	42,483,572	12	Larrès-Fiscal	N292°/47°	4765	1,25E-04	8,63E-06	1011	0,003	1014	0,005	**1026**	0,005	**0,087**	0,236	**34,200**	14,952	Type III
YB_11	−0,284,951	42,483,812	14	Larrès-Fiscal	N318°/66°	4735	1,09E-04	7,16E-06	1015	0,008	1029	0,008	**1046**	0,009	**0,342**	0,282	**39,700**	10,728	Type IV
YB_12	−0,284,306	42,483,719	13	Larrès-Fiscal	/	4720	1,11E-04	4,84E-06	1011	0,003	1050	0,006	**1066**	0,006	**0,625**	0,100	**11,700**	2366	Type V
YB_13	−0,287,500	42,485,185	9	Larrès-Fiscal	N280°/50°	4700	1,44E-04	9,07E-06	1008	0,003	1057	0,006	**1071**	0,006	**0,743**	0,100	**8589**	2396	Type V
YB_14	−0,287,116	42,485,649	13	Larrès-Fiscal	N301°/80°	4645	1,15E-04	1,51E-05	1011	0,008	1022	0,010	**1034**	0,012	**0,317**	0,382	**35,577**	18,373	Type III
YB_15	−0,287,151	42,486,235	13	Larrès-Fiscal	/	4590	1,35E-04	8,40E-06	1010	0,002	1015	0,005	**1026**	0,005	**0,155**	0,243	**36,892**	12,973	Type III
YB_16	−0,286,959	42,486,674	11	Larrès-Fiscal	N301°/60°	4540	1,33E-04	1,44E-05	1010	0,005	1047	0,011	**1061**	0,012	**0,649**	0,170	**12,421**	5330	Type II
YB_17	−0,287,031	42,487,548	10	Larrès-Fiscal	N302°/67°	4460	1,36E-04	6,28E-06	1004	0,002	1052	0,005	**1063**	0,006	**0,852**	0,067	**8390**	2158	Type II
YB_18	−0,286,158	42,488,256	13	Larrès-Fiscal	N305°/55°	4357	1,39E-04	8,53E-06	1009	0,003	1029	0,006	**1040**	0,007	**0,505**	0,131	**21,915**	5972	Type II
YB_19	−0,285,785	42,488,939	11	Larrès-Fiscal	N299°/53°	4277	1,53E-04	3,79E-06	1007	0,003	1045	0,006	**1057**	0,005	**0,739**	0,133	**9727**	3072	Type II

(*continued on next page*)

Table 1 (*continued*)

site	longitude	latitude	n	formation	bedding	d (m)	K_{mean}	σ_{kmean}	L	σL	F	σF	P'	$\sigma_{P'}$	T	σ_T	e23	σ_{e23}	Fabric
YB_20	−0,285,692	42,490,209	13	Larrès-Fiscal	N307°/53°	4155	1,61E-04	7,23E-06	1006	0,003	1033	0,003	**1042**	0,004	**0,678**	0,147	**11,431**	3742	Type II
YB_21	−0,281,859	42,492,151	12	Pamplona	N292°/41°	3800	1,66E-04	5,65E-06	1008	0,003	1032	0,004	**1042**	0,004	**0,599**	0,161	**11,325**	4672	Type II
YB_22	−0,279,809	42,492,827	14	Pamplona	/	3650	1,54E-04	2,69E-05	1010	0,003	1029	0,005	**1041**	0,007	**0,483**	0,121	**13,443**	5211	Type II
YB_23	−0,278,638	42,494,111	12	Pamplona	/	3480	1,66E-04	1,12E-05	1009	0,004	1028	0,008	**1039**	0,008	**0,481**	0,212	**14,533**	2860	Type II
YB_24	−0,276,214	42,495,959	13	Pamplona	N296°/37°	3200	1,56E-04	7,61E-06	1012	0,006	1024	0,004	**1037**	0,007	**0,368**	0,188	**17,323**	4406	Type II
FI_01	−0,121,693	42,499,940	13	Larrès-Fiscal	N300°/63°	900	1,17E-04	7,04E-06	1004	0,002	1067	0,018	**1080**	0,021	**0,874**	0,070	**4108**	1452	Type V
FI_02	−0,122,594	42,499,104	14	Larrès-Fiscal	N300°/88°	1000	1,35E-04	5,43E-06	1014	0,004	1030	0,004	**1046**	0,005	**0,381**	0,170	**6721**	1678	Type IV ?
FI_03	−0,122,895	42,497,667	15	Larrès-Fiscal	N112°/80°	1175	9,68E-05	3,79E-06	1013	0,006	1025	0,006	**1040**	0,005	**0,329**	0,287	**22,987**	7366	Type III
FI_04	−0,122,702	42,494,803	14	Larrès-Fiscal	N112°/65°	1460	1,25E-04	5,28E-06	1010	0,004	1038	0,004	**1051**	0,004	**0,583**	0,144	**11,671**	2838	Type II
FI_05	−0,119,135	42,490,275	12	Larrès-Fiscal	N104°/67°	1660	1,86E-04	8,48E-06	1011	0,004	1035	0,005	**1049**	0,003	**0,507**	0,179	**5867**	2078	Type II
FI_06	−0,167,357	42,444,292	14	Pamplona	N310°/80°	8100	1,54E-04	6,48E-06	1010	0,005	1035	0,008	**1047**	0,008	**0,555**	0,203	**7971**	1744	Type II
FI_07	−0,168,117	42,439,873	13	Larrès-Fiscal	N395°/59°	8540	1,50E-04	1,55E-05	1010	0,007	1017	0,007	**1028**	0,008	**0,290**	0,466	**16,731**	9545	Type III
FI_08	−0,169,205	42,439,487	14	Larrès-Fiscal	N311°/83°	8620	1,12E-04	4,41E-06	1012	0,007	1025	0,008	**1038**	0,010	**0,341**	0,319	**20,200**	10,365	Type III

The next LA 05 and LA 06 sites that lie respectively at 300 m and 500 m from the fault can be identified as a type III magnetic fabric from the roughly triaxial shape and the low degree of anisotropy (Fig. 7). This reinforces our interpretation of a type IV fabric the in the previous sites, with a logical sequence between type V, type IV and type III.

From 500 to 2500 m, the Larrès Marls record a first-order progressive increases of both the P' and T parameters with values characteristics of a type II magnetic fabric that record the transition toward an oblate fabric.

At 3500 m from the thrust fault, the site LA 13 is located approximatively at the hinge of the Yebra anticline and can be reported as a type V magnetic fabric based on higher values in P' and T parameters and the observation of cleavage planes in outcrop.

Between 4000 and 4200 m, the next LA 14 and LA 15 sites sampled in the overturned Larrès Marls are characterized by lower values of both P' (comprised between 1,05–1,06) and T (0.5–0.7) that could be indicative for a type V or a type II magnetic fabric. However, the outcrop rocks fabric displays a strongly deformed pattern, characterized by cleavage planes and calcite veins that is more consistent with a type V fabric.

At least, the Pamplona marls lying in the southern forelimb between 4900 and 5800 m record a high E23 value (>15°) that attest for a poorly defined magnetic foliation. Together with the very low degree of anisotropy and the roughly triaxial shape of the magnetic ellipsoid, this attests for a type III magnetic fabric.

To summarize this cross-section, we can observe a logical sequence of successive fabrics from type V to type II in the footwall of the fault, followed by a type V in the fold hinge, then again type II and type III in the overturned forelimb of the fold. Although the values may overlap, the observation of type III as well as the observation of slaty cleavage in the footwall of the fault and in the heart of the hinge reinforce this evolutionary scheme.

4.3.2. *The Larrede-Yebra composite section*

In the central part of the thrust-fold belt, the Larrede and Yebra subsections gather 39 sites sampled in two transects spreading over 5800 m from the Oturia thrust fault toward the foreland and through the Yebra anticline (Fig. 2B and 8). The Larrede section hosts 12 sites sampled in the Larrès and Pamplona Marls which are underlying the syntectonic Santa Orosia conglomerates in the footwall of the Oturia thrust (Fig. 3B). The Yebra section contains 27 sites sampled in the Larrès and Pamplona Marls across the Yebra anticline in front of the Santa Orosia conglomerates (Fig. 3C). The Larrede-Yebra composite section is dominated by oblate magnetic fabric with some sites of the Larrès Marls displaying equivalent foliation and lineation parameters that reflect the triaxial fabric (Fig. 8A). The four different types of magnetic fabric were identified in the Larrès Marls whereas the Pamplona Marls are characterized by type II and type III magnetic fabrics only (Fig. 8B).

In the first 200 m from the Oturia fault, the site LD 01 and LD 02 sampled in the Larrès Marls are characterized by a type V magnetic fabric as it is evidenced by the high values of anisotropy and shape parameters together with the development of cleavage planes within marls. At approximately 280 m from the fault, a decreasing shift highlights the transition toward a type IV magnetic fabric (Fig. 8C–. D, Fig. 8E).

Between 700 and 2400 m, the sites LD 04 and LD05 in Larrès marls then LD 06 and LD 07 in the Pamplona marls record a decreasing anisotropy as well shape parameters with values respectively comprised between 1.03 - 1.05 and 0.00–0.30. It indicates a type III magnetic fabric. This is consistent with the progressive increase of E23 parameter that reflect the poor expression of a Kmin axis and the magnetic foliation (Fig. 8C–. D, Fig. 8E).

Between 2800 m and 3800 m from the Oturia thrust, the sites LD 08 then LD 09 in Pamplona marls are characterized by T values higher than 0.50 which is indicative for the switch toward a type II magnetic fabric. To the east, the YB 21 to YB 24 sites along the Yebra sections record similarly P′ and T values that are characteristic of a type II magnetic fabric. At this point, the main difference with the western Larrès section

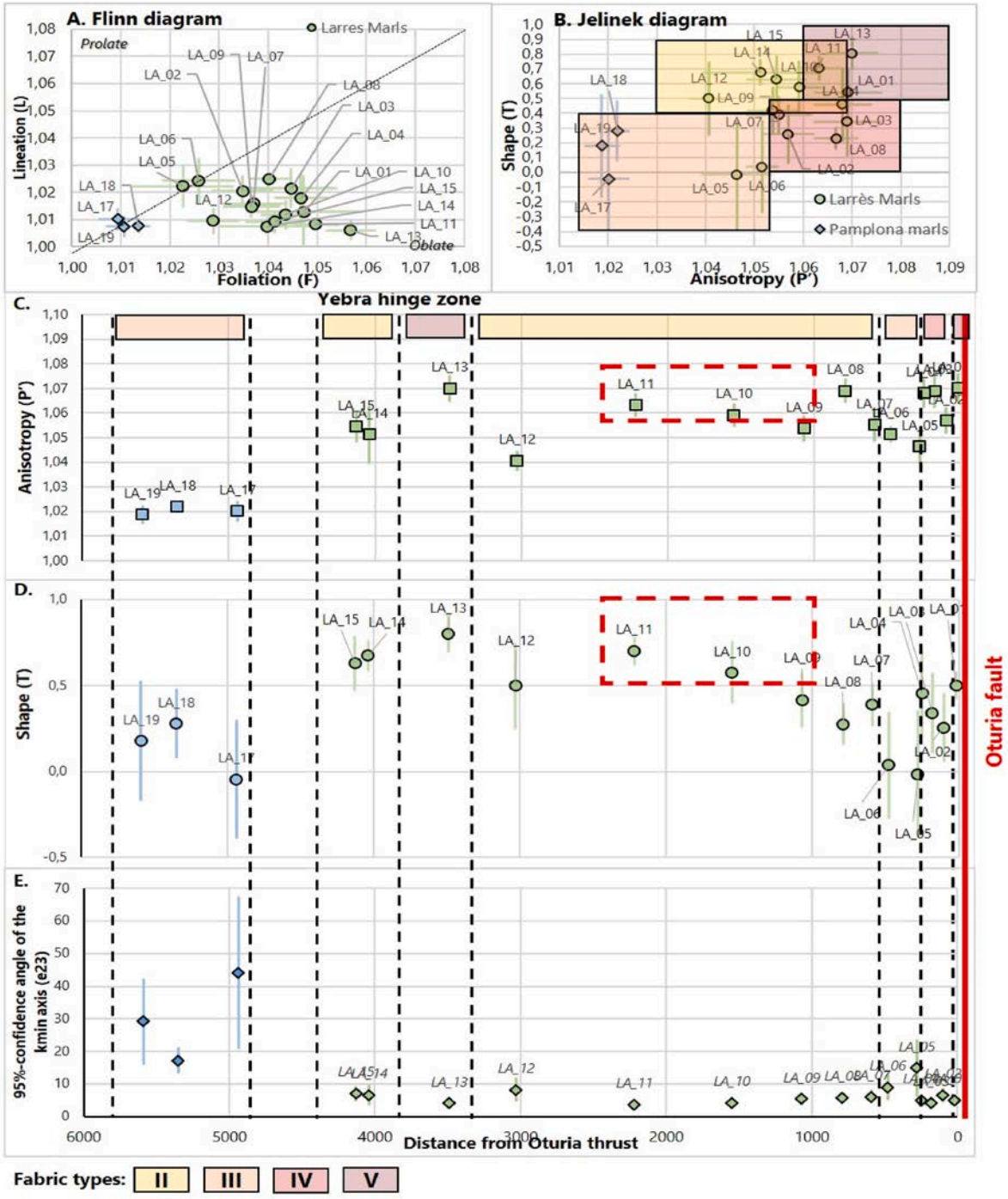

Fig. 7. Results of the AMS analysis in Larrès and Pamplona Marls along the western Larrès section. A) Flinn diagram (Magnetic Lineation (L) versus Foliation (F)). B) Jelinek diagram (Shape (T) versus corrected Anisotropy (P′)). C. Evolution of the Anisotropy from the Oturia fault toward the foreland. D. Evolution of the shape of the magnetic fabric. E) Evolution of the e23 parameter. The red dashed box highlights the P′ and T values in sites lying between 1000 and 2500 m from the thrust fault. (For interpretation of the references to colour in this figure legend, the reader is referred to the Web version of this article.)

is the lower value of both P' and T parameters between the 1500 and 300 m interval. This reflects a persisting triaxial type III fabric in the marls lying beneath the Santa Orosia conglomerates (Fig. 8C and D).

Between 4100 and 4550 m, the sites YB 20 to YB 16 sampled in Larrès Marls can be interpreted as a type II magnetic fabric. This is consistent with the structurally and stratigraphically equivalent LD 10 site in the Larrede transect.

Between 4550 and 4650, the next two sites YB 15 and YB 14 strongly are characterized by very low anisotropy (P' between 1.02 and 1.04) and shape parameters (T lower than 0.4). Correlating with a net increase in the E23 parameter, this indicates a poorly expressed magnetic foliation characteristic of the type III magnetic fabric.

In contrast, the sites LD 11, YB 13 and YB 12 that lie in the hinge of the Yebra anticline are characterized by very strong T and P′ values, that range respectively from 0.60 to 0.90 and 1.55 to 1.70. It can be related to a type V fabric, consistently with the cleavage pattern observed in the outcrop structural fabric (Fig. 6E–G). However, the strongly decrease in both P′ and T values in next YB 11 and YB 10 sites records the sharp transition toward a type III magnetic fabric along a 50 m-large interval. They are followed southward by the site YB 09 (4800 m) where very

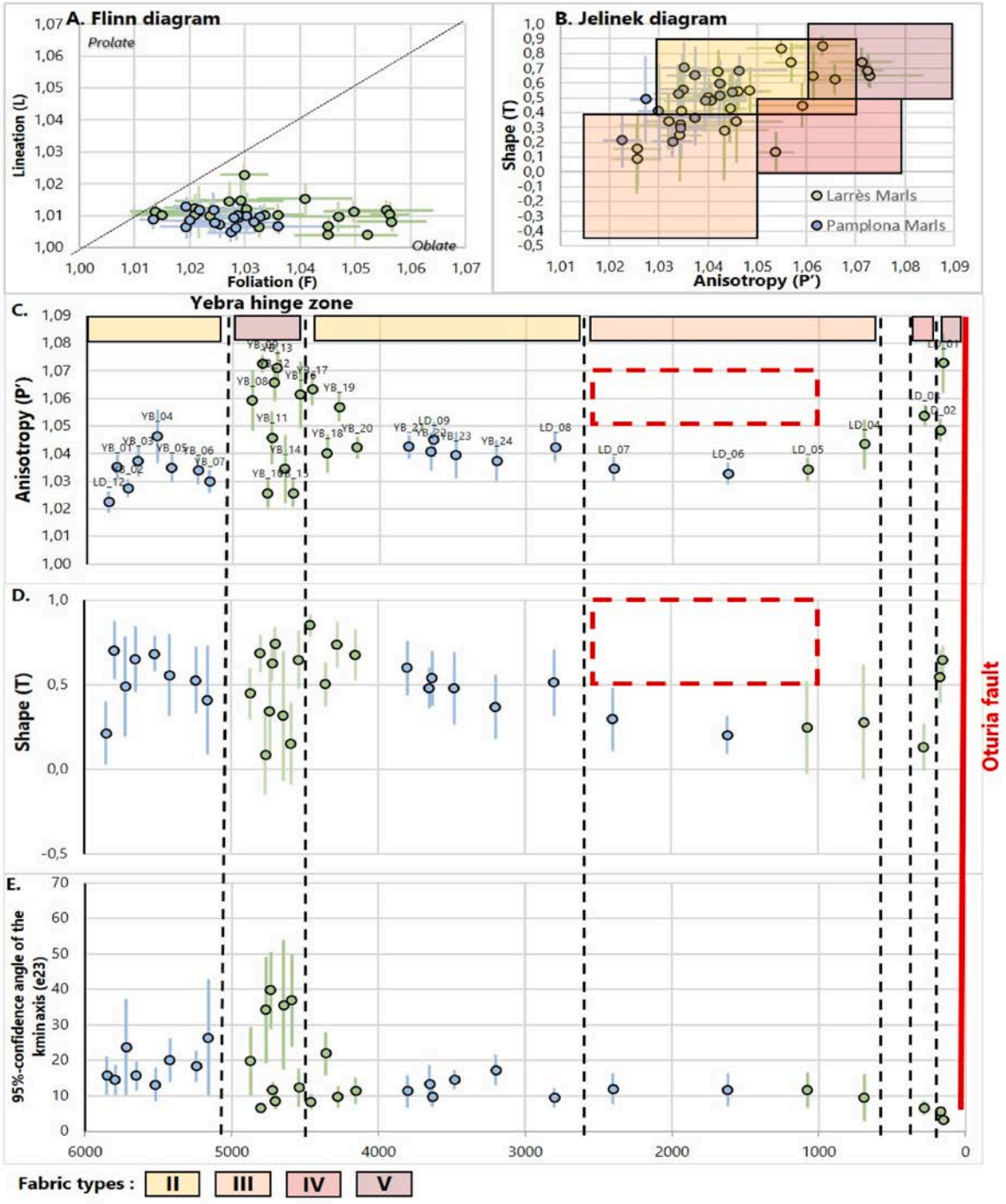

Fig. 8. Results of the AMS analysis in Larrès and Pamplona Marls along the central Larrede-Yebra composite section. A) Flinn diagram (Magnetic Lineation (L) versus Foliation (F)). B) Jelinek diagram (Shape (T) versus corrected Anisotropy (P′)). C. Evolution of the Anisotropy from the Oturia fault toward the foreland. D. Evolution of the shape of the magnetic fabric. E) Evolution of the e23 parameter. The red dashed box highlights the P′ and T values in sites lying between 1000 and 2500 m from the thrust fault. (For interpretation of the references to colour in this figure legend, the reader is referred to the Web version of this article.)

high P′ and T values indicates a type V magnetic fabric, then by the site YB 08 (4870 m) where the slight decrease in both P′ and T parameters reflect the change to a type IV fabric. To resume, the hinge of the Yebra anticline is characterized by highly oscillating sites P' and T values in 50 m–100 m-large intervals that record alternance of narrow bands of type V, type IV and type III magnetic fabrics.

Finally, the sites YB 07 to YB 01 sampled in the Pamplona marls between 5000 m and 6000 m are characterized by a roughly homogenous anisotropy with P′ values that range between 1.02 and 1.05 and an oblate shape recorded by positive T values (0.40–0.80). Together, these indicate a type II magnetic fabric. In contrast, the structurally equivalent site LD 12 fabric in the Larrede transect shows a very low anisotropy (P'<1.03) correlated with E23 > 20° that is indicative for a type III fabric.

4.3.3. *The Fiscal-Gilué section*

In the eastern part of the thrust-fold belt, the Fiscal-Gilué section is represented by eight sites sampled along two <1000 m long transects on

either side of the Peña Cancias (Figs. 2B and 10). The northern Fiscal sub-section is composed of five sites sampled in the Larrès-Fiscal Marls outcropping in the footwall of the Oturia thrust. The southern Gilué sub-section is composed of three sites sampled in the Larrès and Pamplona marls at the eastern end of the Yebra anticline. Oblate magnetic fabrics are dominating although some sites show a more triaxial shape (Fig. 10A). Three types of magnetic fabrics were recognized from the Oturia thrust toward the foreland (Fig. 10B).

The FI 01 site is located approximatively 900 m southward of the Oturia fault. It has been sampled in a lowermost horizon of the Larrès-Fiscal marl that are structurally lie below the allochthonous Hecho turbidites. It is characterized by a strong anisotropy as well as shape parameters that indicate together a type V magnetic fabric (Fig. 10C and D).

At 1000 m the site FI 02 which shows a sharp decrease in both anisotropy and shape parameters that is indicative for the transition toward a type IV (or maybe a type III) magnetic fabric. At 1200 m, the increase of E23 parameters suggest that the site FI 03 is characterized by a type III fabric (Fig. 10E). From 1400 m to 1700 m, sites FI 04 and FI 05 are characterized by a type II following the P' and T values. In summary, the Fiscal sub-section shows a global change from a type V fabric to a type II fabric over a distance of 1500 m from the fault toward the foreland. This evolution is corroborated by the observation of a slaty cleavage in the footwall of the fault that disappears southward.

The second area is located at the periclinal termination of the Yebra anticline between 8000 m and 8700 m from the thrust fault. The site FI 06 sampled in the Pamplona Marls is characterized by equivalent values of the P', T and E23 parameter attesting for a type II fabric. Further south, between 8500 m and 8700 m the Larrès Marls lying in the fold hinge (site FI 08 and FI09) are characterized by a type III magnetic fabric.

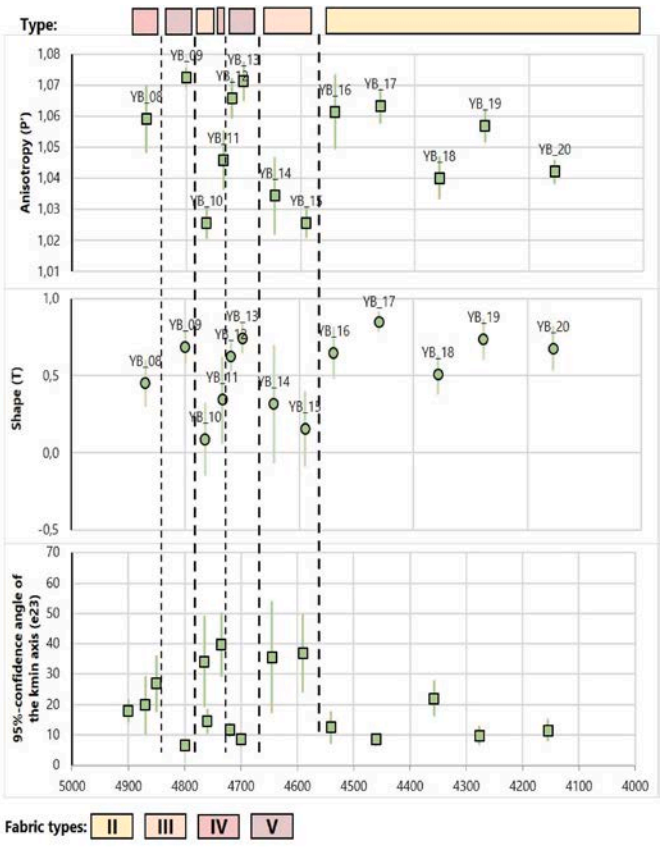

Fig. 9. Short-scale evolution of anisotropy parameters and magnetic fabrics within the hinge of the Yebra anticline.

4.4. Along-strike correlation of magnetic fabrics and regional synthesis

At the first order, the studied sections show a similar trend in the succession of magnetic fabrics, that can be described as: (i) the evolution from type V and type IV fabrics in the footwall of the Oturia thrust to type III then type II toward the foreland; ii) mixed type V – type III fabrics in the Larrès Marls lying in the Yebra fold hinge and iii) type III-type II fabrics in the Pamplona Marls of the southern overturned forelimb (Fig. 10).

Based on the correlation of the successive intervals between the three sections, we propose a synthetical map of the magnetic fabrics in the Larrès and Pamplona marls in the eastern Jaca basin (Fig. 11). At the regional scale, the distribution of the magnetic fabric corresponds to successive bands trending subparallel to the main structures, with some along-strike variations either in type of magnetic fabrics or width of the magnetic domain.

The northernmost domain corresponds to a type V - type IV magnetic fabrics band that extends between 0 and 300 m along the Oturia thrust fault in all sections. It correlates with the occurrence of a slaty cleavage within marls (Fig. 6A and B, Fig. 11), similarly to what was described in the footwall of the Leyre thrust at the Siguès area (Boiron et al., 2020).

It is followed southward by a type III domain (Fig. 6C) whose the overall width is variable between the four sections. In the western Larrès as well as in the eastern Fiscal areas, type III magnetic fabric extends approximatively 300 m in the footwall of the Oturia thrust (Figs. 7 and 11). In the central Larrede-Yebra composite section, the type III magnetic fabrics band is wider and extends over more than 2000 m from the thrust fault beneath the syn-tectonic Santa Orosia conglomerates (Figs. 8 and 11). This trend, supported by 4 successive sites, suggests the influence of a 2nd-order mechanism that locally modify the magnetic fabric record within marls.

Beyond, the type II magnetic domain is homogeneous in the western and central section, extending 2500 m southward as an area corresponding approximatively to the southern part of the Orosia-Cancias depositional syncline (Fig. 6D). In the eastern Fiscal section, the extent of the type II magnetic domain cannot be estimated because of the outcropping massive Cancias conglomerates. Nevertheless, the presence of a type II fabric on either side suggests a sole continuous, 7000 m-wide band. The overall evolution of magnetic fabrics in the footwall of the Oturia thrust is thus similar to what was described in the footwall of the Leyre thrust in the western Jaca basin (Boiron et al., 2020; Gracia-Puzo et al., 2021).

To the south, the hinge of the Yebra anticline is dominated by the type V and type III magnetic fabrics which are associated with the occurrence of cleavages in marls (Fig. 6E, F, G, Fig. 11). At the western Larrès and Larrede sections, only one site was sampled within the fold hinge which is not sufficient to discard the occurrence of type III fabric. Along the central Yebra section, the dominating type V fabric alternates with type III developed as 100 m-scale bands. Further east in the Fiscal section, the fold hinge is dominated by a type III magnetic fabric with no evidence of type V. This eastward change in magnetic fabric along the strike of the fold can be correlated with a change in the fold geometry. To the east where the type III fabric dominates, the fold geometry is upright with two steeply dipping normal limbs; by contrast, it is overturned with a reverse forelimb where the type V fabric are dominating.

The southernmost domain corresponds to overturned Pamplona Marls in the forelimb of the Yebra anticline that are dominated by type II and type III fabrics. In the central Yebra section, the Pamplona marls are characterized by an 1 km-wide band of dominating type II fabrics (Figs. 6H and 11) whereas in the western Larrès and Larrede sections, the Pamplona marls are characterized by a 1-km wide domain with type III fabric.

5. Discussion

The study of magnetic fabric within Larrès and Pamplona Marls

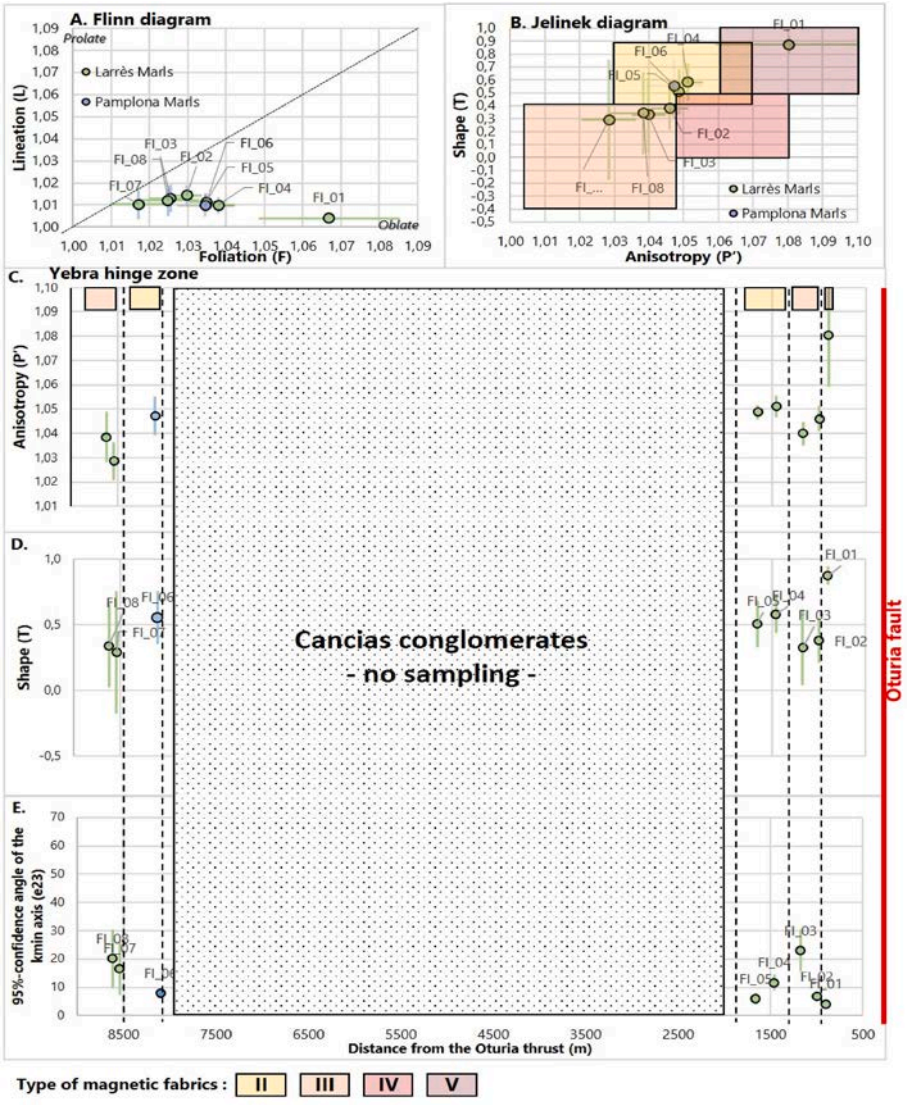

Fig. 10. Results of the AMS analysis in Larrès and Pamplona Marls along the eastern Fiscal section. A) Flinn diagram (Magnetic Lineation (L) versus Foliation (F)). B) Jelinek diagram (Shape (T) versus corrected Anisotropy (P')). C. Evolution of the Anisotropy from the Oturia fault toward the foreland. D. Evolution of the shape of the magnetic fabric. E) Evolution of the e23 parameter.

evidences both regional and local variations of magnetic fabrics in the study area. Whereas the first could be related to regional shortening and tectonic processes, the second necessary involve a superimposed local controlling factor. Based on these results, we discuss here the influence of thrusting and folding, as well as the syn-tectonic sedimentation, on the matrix deformation within the Larrès and Pamplona marls.

5.1. *Effect of thrusting and folding on the magnetic fabrics*

At the first order, the regional pattern of the magnetic fabrics corresponds to N110°-N130° bands striking parallel to the Oturia fault and the Yebra anticline axis (Fig. 11). This argues in favour of a relationship between the evolution of magnetic fabrics and the deformation of the clay matrix related to thrusting and folding.

5.1.1. *Matrix deformation of marls in the footwall of the Oturia thrust*

In the footwall of the Oturia thrust, the magnetic fabric is distributed as an asymmetric succession from the type V to the type II toward the foreland (Fig. 11), similarly to what is documented in the footwall of the Leyre thrust in the western Jaca basin (Boiron et al., 2020; Gracia-Puzo et al., 2021). Here the succession of magnetic fabrics was interpreted as recording the evolution of the strain gradient from the fault toward the foreland in response to the Leyre thrusting. We propose therefore that the evolution of magnetic fabrics in the footwall of the Oturia fault records an overall matrix strain gradient following a four-step model in response to horizontal contraction and shearing during thrusting (Fig. 12A).

The type V magnetic fabric lying closely from the thrust fault is interpreted as a tectonic fabric in which the magnetic foliation reflects the re-orientation of clay particles by shearing beneath the fault plane. This is recorded by the development of a strong slaty cleavage along the thrust fault. The weakly oblate to triaxial type IV magnetic fabric highlights the transition toward an intermediate fabric in which the decreasing controlled by a tectonic foliation. The following triaxial type III fabric records the competition between bedding-related and tectonic-controlled magnetic foliation (Saur et al., 2020). Beyond, the oblate type II fabric records the preservation of a bedding-controlled magnetic foliation. However, the occurrence of fractures in outcrop (Fig. 6D) and the large range of P' and T values indicate an incipient matrix strain that could be related to the LPS. This succession of magnetic fabrics in the footwall of the Oturia fault is interpreted as recording an overall increase of the internal deformation related to thrusting (Fig. 12A). The

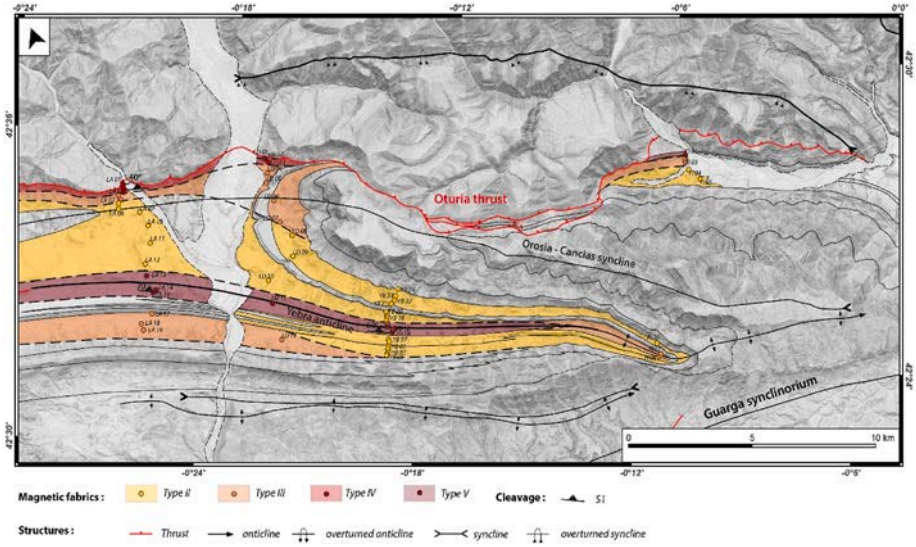

Fig. 11. Map of magnetic fabrics distribution in the Larrès and Pamplona Marls of the eastern Jaca basin.

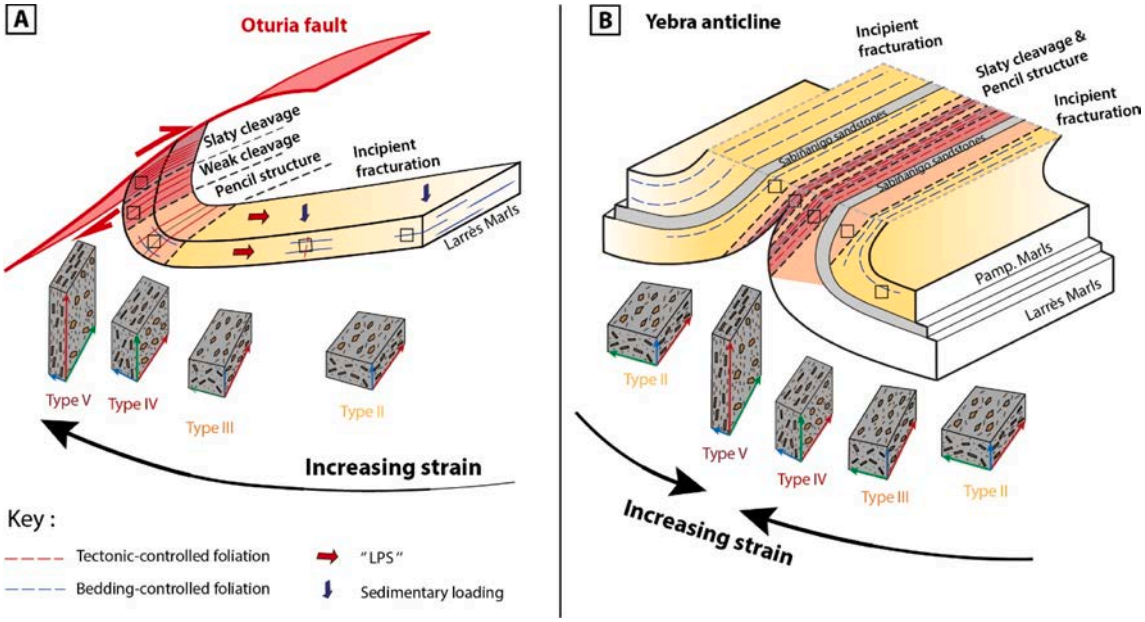

Fig. 12. Model of magnetic fabrics evolution in the footwall of the Oturia fault (A) and across the Yebra anticline (B).

similarity of the deformation gradient in the footwall of the Leyre and Oturia faults suggests that the mechanism at work is the same. In the Sigues area, the Leyre fault probably propagated into a deeper part, since the marls experienced a burial temperature of the order of 150 °C or more (Boiron et al., 2020). Along the Oturia fault, the maximum burial temperature is lower (<100°C, Labaume et al., 2016). It is therefore possible that the behaviour of fault propagation is not the same in a ductile level such as marl. The zone of a thrust is generally limited to a few meters, but not a gradient over several hundred meters). Boiron et al. (2020) have proposed a trishear model of fault propagation. The triangular zone at the fault apex acts as a shear prism. Our data do not confirm or refute this trishear model, but indicate that the propagation mode of the Oturia fault generated the matrix deformation of marls over several hundred meters.

5.1.2. *Matrix deformation of marls related to folding*

The Yebra anticline is a special detachment fold, since the hinge is welded, bringing the Larrès marls of both limbs into contact (Figs. 2C and 3C). Three types of magnetic fabrics dominate the fold area, with a roughly symmetric distribution from type II in the backlimb to alternating type V - type III fabrics within the fold hinge and dominating type II fabrics in the overturned forelimb. In details, the Larrès and Pamplona Marls in the backlimb record exclusively type II fabrics whereas in the forelimb the Pamplona Marls lying in the western part records also some type III fabrics (Figs. 10 and 12B). In contrast, the Larrès Marls within the fold hinge are marked by an of the succession of type III, type IV and type V fabrics distributed as 100 m-wide alternating bands over a distance of 500 m (Figs. 9 and 12B). This organisation is similar to that one described by Larrasoaña et al. (1997) in a parallel section crossing the Yebra anticline. Authors showed that the magnetic fabrics observed in the different part of the fold was resulting of various deformation mechanism, from pure shear to simple shear that occurred in the successive stages of the fold growth, from the early LPS stage to folding and late stage fold tightening (Lacombe et al., 2021; Larrasoaña et al., 1997).

According to these models we interpret the oblate type II magnetic fabric observed in both limbs of the Yebra anticline as resulting from the re-orientation of clay particle in response to pure shear horizontal contraction during the Layer Parallel Shortening stage.

Type III fabrics in the fold hinge are interpreted as resulting from the re-orientation of the clay particles in response to pure shear, tangential-longitudinal compression within the inner hinge in response to buckling during the folding. Type III fabrics in the overturned forelimb are interpreted as related to simple-shear mechanisms in response to bed-to-bed flexural slip during the fold overturning, similarly to what happens in the footwall of thrust faults.

Within the fold hinge, type V magnetic fabrics distributed as thin, <100 m wide, bands are more difficult to interpret as they could be related to different deformation processes. First, the occurrence of slaty cleavage within (Fig. 6) could suggest that type V fabrics developed by pressure-solution processes. These macro-scale pressure-solution bands could develop during LFST as a response to the increase of horizontal compressive strain during the hinge flattening (Lacombe et al., 2021; Larrasoaña et al., 1997). Alternatively, type V fabrics could be related to the development of shear bands within the shaly fold hinge. In shale-dominated detachment zones (Morley et al., 2017, 2018), the internal deformation of shale units results in the complex and multi-scale imbrication of scaly fabrics, S–C fabrics and cleavages zone that form duplexes within the fold hinge (Morley et al., 2017) These are delimited by principal displacement zones (PDZs) that correspond in fact to shear bands (Morley et al., 2018). Following this model, type III fabrics could be representative for the matrix deformation in duplexes that alternated with preferential shear zone recording trough the development of type V fabrics (Morley et al., 2017, 2018).

Whatever the involved deformation mechanism, the pattern of mixed type III and type V magnetic fabric within the fold hinge highlights the complete annealing of the initial sedimentary fabric and, therefore, a symmetrically increasing strain gradient from both limbs toward the fold hinge. This shed light on the localization and extension of the main strain zone in folded area which is not obvious from field observations. In the case of the Yebra shale-dominated detachment fold, the domain of maximum strain is located within the fold hinge and extends approximatively 500 m.

5.2. *Influence of the syn-tectonic sedimentation on the matrix deformation of marls*

Although the distribution of magnetic fabrics in the Larrès and Pamplona Marls is similar at the regional scale from the Oturia fault toward the foreland, some 2nd-order, local variations can be evidenced between the four sections. The major feature corresponds to the varying

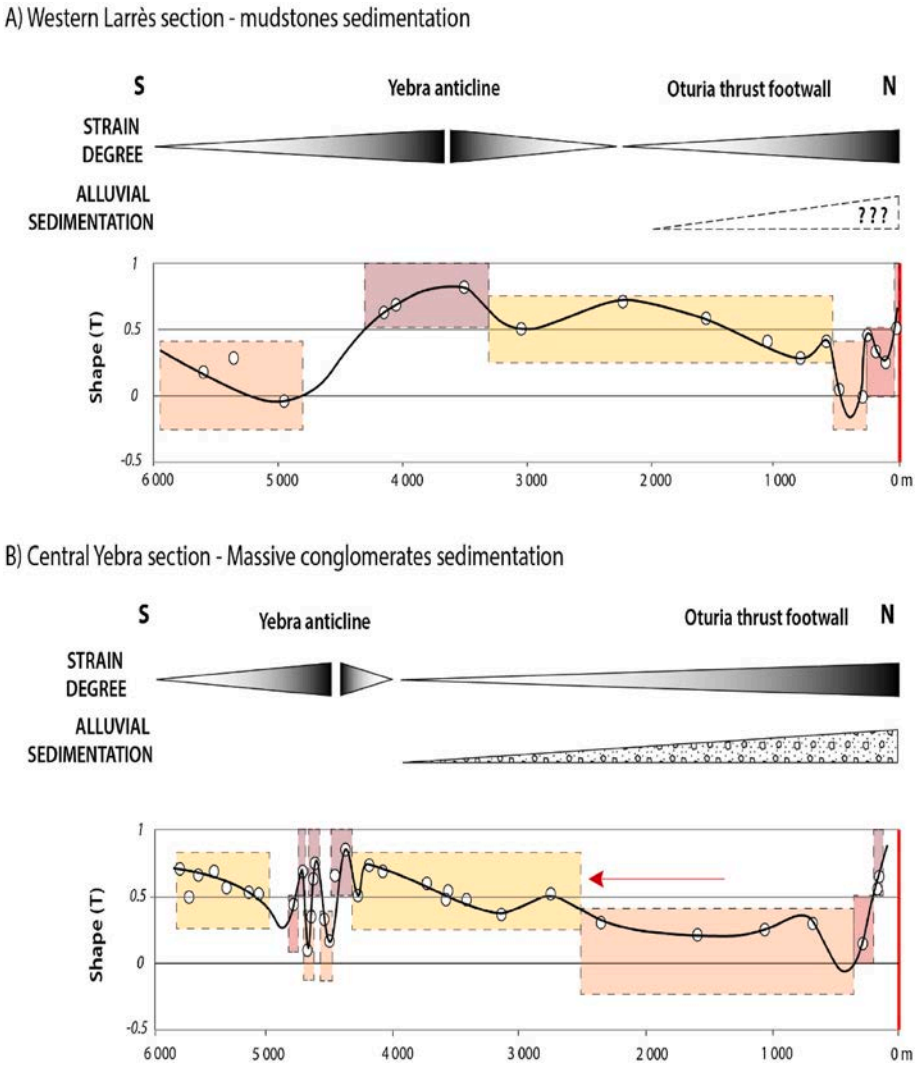

Fig. 13. Evolution of the shape of the magnetic fabric between the eastern Larrès section (A) and the central section (B). The red arrow in section B highlights the varying distance for the reappearance of a strongly oblate shape (T > 0.5) in relation to section A. (For interpretation of the references to colour in this figure legend, the reader is referred to the Web version of this article.)

width of the type III magnetic fabric in the footwall of the Oturia thrust (Figs. 11 and 13). In the central Larrede-Yebra composite section, the Pamplona Marls lying in the Orosia-Cancias syncline are characterized by the widening (>2 km) of the type III magnetic domain. This contrasts with the Larrès and Fiscal sections, where the extent of type III magnetic fabrics in the Larrès marls is shorter (600 m). Furthermore, it has been shown that the magnetic fabrics of marls in the Orosia Cancias syncline records the matrix deformation related to the early LPS then syn-sedimentary thrusting and folding events during late Bartonian and Priabonian. The central zone therefore evidences an extended matrix deformation of the Pamplona Marls towards the foreland, which is not observed in the other two sections. This variation can be related to a 2nd-order, local factor enhancing the matrix deformation during thrusting and folding. At this time in the western and eastern parts of our study area, the sedimentary environment corresponds to a floodplain where are deposited mainly red siltstones and mudstones (Fig. 3D). In contrast, the central area is characterized by the development of an alluvial fan and the deposition of more than 500 m-thick massive conglomerates. We propose therefore that the type III domain widening beneath the Santa-Orosia conglomerates records an increase of the matrix deformation in marls lying beneath the syn-tectonic alluvial conglomerates during their deposition.

Furthermore, it seems that the timing of conglomerates sedimentation versus the tectonics event responsible for the matrix deformation is important. In the eastern Fiscal section, the deposition of the 1000 m-thick Laguarta-Cancias conglomerates sequence that is, in this area, subsequent to thrusting (Fig. 3D), does not appear to have modify the extent of the magnetic fabrics in the footwall of the Oturia fault. On the basis of these observations, we propose that the extent of the matrix deformation in the fold and thrust belt may be affected by the nature and timing of alluvial sedimentation.

5.3. *Integration in the tectono-sedimentary scheme of the eastern Jaca basin*

The AMS data presented here evidenced the effect of thrusting and folding as well as the influence on the syn-tectonic sedimentation on the matrix strain record within the Larrès-Fiscal and Pamplona Marls formation. We propose therefore to integrate this results in the tectono-sedimentary framework of the Jaca basin.

From the syn-sedimentary geometries recorded in the deltaic to conglomerate units, it is possible to decomposed the tectono-sedimentary evolution of the study are in three successive stages. First is the deposition of the shallow-marine Pamplona Marls and Atarès

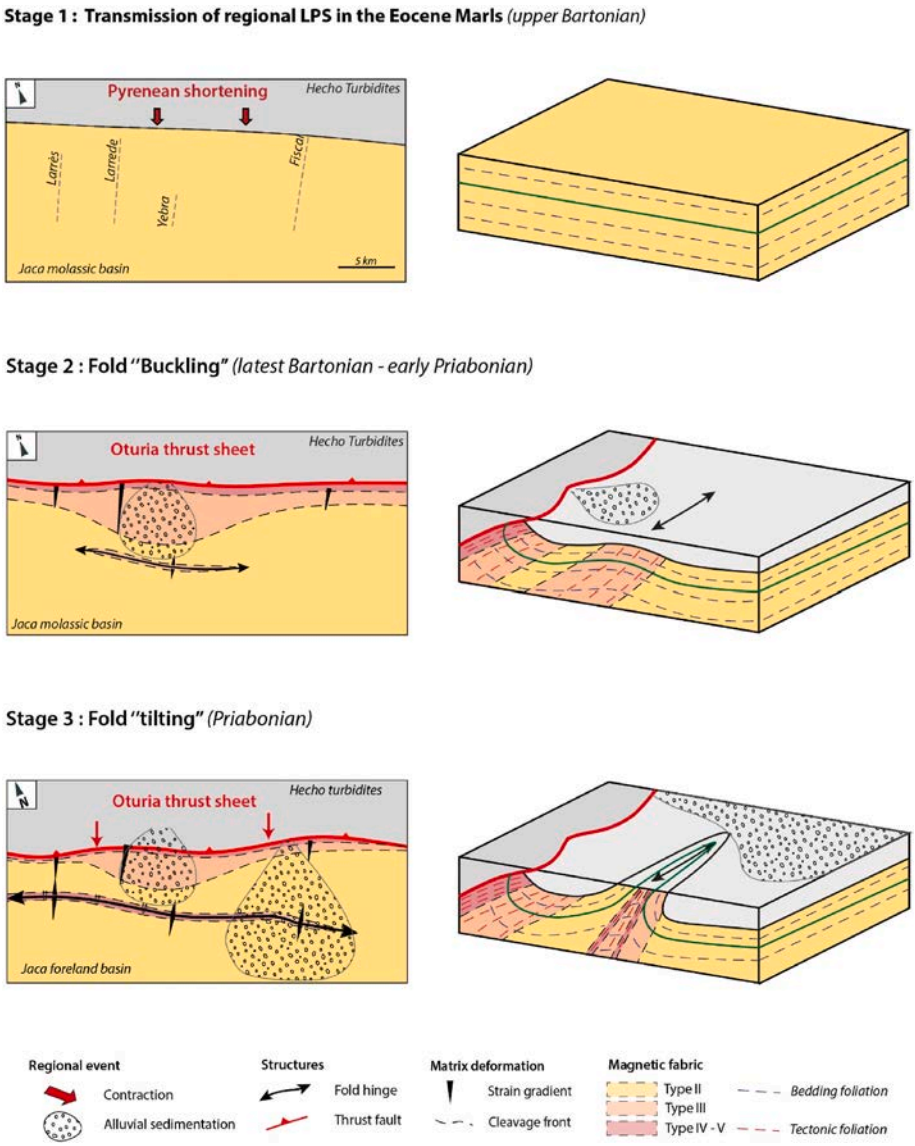

Fig. 14. Sketch of the main stages of the matrix deformation during the tectono-sedimentary evolution of the eastern Jaca basin.

Sandstones formations during Bartonian, that is coeval with the onset of the Oturia thrust as evidenced by the northward thinning of the whole sequence (Fig. 3B). Second is the deposition of the Santa Orosia conglomerates during late Bartonian, that is concomitant with thrusting along the Oturia fault to the north and the early growth of the Yebra anticline to the south. During Priabonian, the deposition of the Laguarta-Cancias conglomerates is coeval with the continuous thrusting of the Hecho turbidites southward on the lower Santa Orosia conglomerates (Fig. 3B–D). On the southern limb of the Yebra anticline, progressive unconformities within the Laguarta-Cancias conglomerates evidence the tilting of the fold toward the south and the overturning of the Santa-Orosia conglomerates in the anticline forelimb (Fig. 3C).

Within the Larrès and Pamplona Marls, the first stage of matrix strain corresponds to the LPS that resulted in the development of the type II fabric. This is interpreted to be linked with the onset of the Oturia thrust to the north soon after the marls deposition during upper Bartonian time (Fig. 14).

Following the tectono-sedimentary evolution of the study area, the second stage of matrix deformation is related to thrusting along the Oturia fault to the north and the early folding of the Yebra anticline to the south. In the central part of the study area, this is coeval with the deposition of the Santa Orosia conglomerates between both structures, whereas the deposition of floodplain mudstones dominated to the east and to the west. In the footwall of the Oturia thrust, the development of type V to type II magnetic fabrics toward the foreland is interpreted as linked to this period. In the western and eastern section, this succession occurs in a few hundred meters (<1000 m) from the fault and records the overall decrease of the matrix strain toward the foreland in a distance roughly similar to what was described in the western Jaca basin (Boiron et al., 2020; Gracia-Puzo et al., 2021). In the central part of the study area, this gradient appears to be more diffuse as intermediate, type III magnetic fabrics extend beyond 2000 m from the fault. This suggest that the matrix strain propagates further south within the marls lying beneath the Santa Orosia conglomerates and is interpreted to reflect the local influence of the syn-tectonic sedimentation (Figs. 11 and 14). To the south, the early growth of the Yebra anticline is interpreted to be responsible for the development of the type III fabrics within the Larrès Marls in the hinge zone, that superimposed to the inherited type II fabrics from the former LPS stage.

The latest stage of matrix deformation in marls can be related to the fold hinge tightening and tilting that occur synchronously with the deposition of the Laguarta-Cancias during Priabonian. The horizontal compressive stresses related to flattening of the hinge zone is interpreted to be responsible for the development of the type V fabric as < 100 m large bands superimposed to the inherited type III fabric from the early fold growth phase. At this time, the ongoing thrusting along the Oturia fault could be responsible for a low southward migration of the magnetic fabric types.

6. Conclusion

In this study, we used the anisotropy (P') and shape (T) AMS parameters to highlight the regional pattern of magnetic fabrics recorded within the Larrès and Pamplona Marls of the eastern Jaca basin. Four types of magnetic fabrics characterized by oblate to triaxial shapes, were defined along the four studied sections crossing the main regional structures. At the first order, marls recorded a gradient from a type V magnetic fabric in the footwall of the Oturia thrust to a type II magnetic fabric towards the foreland. In the Yebra anticline, the magnetic fabrics change from dominating type II with some type III in both fold limbs, to alternating types III, IV and V within the fold hinge. These magnetic fabrics are interpreted as the result of variable degree of matrix deformation related to various deformation mechanisms during thrusting and folding events. Areas of maximum matrix deformation are located first in a <1000 m wide band that underlines the Oturia fault and second in a 1000 m wide domain in the hinge of the Yebra anticline. Between these two areas, the matrix deformation in marls is weaker.

The regional correlation of magnetic fabrics between the four sections highlights second-order, along-strike variations that can be related to a change in the matrix strain record. As both sedimentary burial and tectonic processes can be considered homogeneous throughout the study area, we interpret this as related to the influence of the syn-tectonic sedimentation. Beneath the Santa Orosia conglomerates, types II fabrics extend more than 200 m from the Oturia fault, by contrast with the eastern and western sections. We interpret this as a propagated matrix deformation of marls toward the foreland due to the deposition of a thick layer of conglomerates above.

CRediT authorship contribution statement

R.L. Menzer: Conceptualization, Investigation, Visualization, Writing – original draft, Writing – review & editing. **C. Bonnel:** Conceptualization, Funding acquisition, Investigation, Supervision, Validation, Visualization, Writing – original draft, Writing – review & editing. **F. Gracia-Puzo:** Conceptualization, Investigation, Methodology, Visualization. **C. Aubourg:** Conceptualization, Investigation, Methodology, Validation, Writing – original draft, Writing – review & editing.

Declaration of competing interest

The authors declare that they have no known competing financial interests or personal relationships that could have appeared to influence the work reported in this paper.

Data availability

Data will be made available on request.

Acknowledgements

The authors thank very much Pr. François Baudin (Université « Pierre et Marie Curie » - Paris VI) for its contribution through RockEval 6 analyses at ISTeP and its comments concerning results. We thank M-P. Isaure (UPPA) for the help in X-ray diffraction measurement and analysis and C. Carvallo (UPMC) for VSM measurements. We thank very much R. Soto (IGME) and an anonymous reviewer for their numerous and constructive feedbacks that greatly helped to improve the original manuscript. We thank also Damien Huyghes (MinesParisTech, Université PSL) and Jean-Paul Callot (LFCR, Université de Pau et des Pays de l'Adour) for their remarks concerning our methodology and results during this PhD work. We are grateful to UPPA for the financial support of this study trough the E2S grant.

Appendix A. Supplementary data

Supplementary data to this article can be found online at https://doi.org/10.1016/j.jsg.2024.105114.

References

Andrieu, S., Saspiturry, N., Lartigau, M., Issautier, B., Angrand, P., Lasseur, E., 2021. Large-scale vertical movements in Cenomanian to Santonian carbonate platform in Iberia: indicators of a Coniacian pre-orogenic compressive stress. BSGF - Earth Sci. Bull. 192, 19. https://doi.org/10.1051/bsgf/2021011.

Arenas, Millan, Pardo, Pocovi, 2001. Ebro Basin continental sedimentation associated with late compressional Pyrenean tectonics(north-eastern Iberia): controls on basin margin fans and fluvial systems. Basin Res. 25.

Aubourg, C., Rochette, P., Bergmüller, F., 1995. Composite magnetic fabric in weakly deformed black shales. Phys. Earth Planet. In. 87, 267–278. https://doi.org/10.1016/0031-9201(94)02962-B.

Aubourg, C., Rochette, P., Stéphan, J.-F., Popoff, M., Chabert-Pelline, C., 1999. The magnetic fabric of weakly deformed Late Jurassic shales from the southern subalpines chains (French Alps): evidence for SW-directed tectonic transport

direction. Tectonophysics 307, 15–31. https://doi.org/10.1016/S0040-1951(99)00116-X.
Aubourg, C., Rochette, P., Vialon, P., 1991. Subtle stretching lineation revealed by magnetic fabric of Callovian-Oxfordian black shales (French Alps). Tectonophysics 185, 211–223. https://doi.org/10.1016/0040-1951(91)90445-X.
Aubourg, C., Smith, B., Bakhtari, H., Guya, N., Eshragi, A., Lallemant, S., Molinaro, M., Braud, X., Delaunay, S., 2004. Post-Miocene shortening pictured by magnetic fabric across the Zagros-Makran syntaxis (Iran). In: Special Paper 383: Orogenic Curvature: Integrating Paleomagnetic and Structural Analyses. Geological Society of America, pp. 17–40. https://doi.org/10.1130/0-8137-2383-3(2004)383[17:PSPBMF]2.0.CO;2.
Averbuch, O., Frizon de Lamotte, D., Kissel, C., 1992. Magnetic fabric as a structural indicator of the deformation path within a fold-thrust structure: a test case from the Corbieres (NE Pyrenees, France). J. Struct. Geol. 14, 461–474.
Barnolas, Chiron, A., 1996. Synthése géologique et géophysique des Pyrénées. 1: introducion, Géophysique. In: M, B.R.G. (Ed.), Cycle Hercynien. BRGM, Orléans.
Barnolas, A., Teixell, A., 1994. Platform sedimentation and collapse in a carbonate-dominated margin of a foreland basin (Jaca basin, Eocene, southern Pyrenees). Geology 22, 1107–1110.
Barrier, L., Nalpas, T., Gapais, D., Proust, J.N., 2013. Impact of synkinematic sedimentation on the geometry and dynamics of compressive growth structures: insights from analogue modelling. Tectonophysics 608, 737–752.
Barrier, L., Nalpas, T., Gapais, D., Proust, J.N., Casas, A., Bourquin, S., 2002. Influence of syntectonic sedimentation on thrust geometry. field examples from the Iberian Chain (Spain) and analogue modelling. Sediment. Geol. 146 (1–2), 91–104.
Behar, F., Beaumont, V., De, B., Penteado, H.L., 2001. Rock-eval 6 technology: performances and developments. Oil & Gas Science and Technology - Rev. IFP 56, 111–134. https://doi.org/10.2516/ogst:2001013.
Blouin, A., Sultan, N., Pierron, A., Imbert, P., Callot, J., 2020. Evolution model for the absheron mud volcano: from stratified sediments to fluid mud generation. J. Geophys. Res. Earth Surf. 125 https://doi.org/10.1029/2020JF005623.
Boiron, T., Aubourg, C., Grignard, P.-A., Callot, J.-P., 2020. The clay fabric of shales is a strain gauge. J. Struct. Geol. 138, 104130 https://doi.org/10.1016/j.jsg.2020.104130.
Borradaile, G.J., Henry, B., 1997. Tectonic applications of magnetic susceptibility and its anisotropy. Earth Sci. Rev. 42, 79–93.
Borradaile, G.J., Tarling, D.H., 1981. The influence of deformation mechanisms on magnetic fabrics in weakly deformed rocks. Tectonophysics 77, 151–168.
Borradaile, J., Jackson, M., 2004. Anisotropy of Magnetic Susceptibility (AMS): Magnetic Petrofabrics of Deformed Rocks, vol. 238. Geological Society, London, Special Publications, pp. 238–360.
Brandes, C., Tanner, D.C., 2014. Fault-related folding: a review of kinematic models and their application. Earth Sci. Rev. 138, 352–370. https://doi.org/10.1016/j.earscirev.2014.06.008.
Branellec, M., Callot, J.-P., Aubourg, C., Nivière, B., Ringenbach, J.-C., 2015. Matrix deformation in a basement-involved fold-and-thrust-belt: a case study in the central Andes, Malargüe (Argentina). Tectonophysics 658, 186–205. https://doi.org/10.1016/j.tecto.2015.07.022.
Caja, M.A., Marfil, R., Garcia, D., Remacha, E., Morad, S., Mansurbeg, H., Amorosi, A., Martínez-Calvo, C., Lahoz-Beltrá, R., 2010. Provenance of siliciclastic and hybrid turbiditic arenites of the Eocene Hecho Group, Spanish Pyrenees: implications for the tectonic evolution of a foreland basin. Basin Res. 22, 157–180. https://doi.org/10.1111/j.1365-2117.2009.00405.x.
Caldera, N., Teixell, A., Griera, A., Labaume, P., Guardia, M., 2023. Alpine ductile deformation of the upper iberian collided margin (Eaux-Chaudes massif, west-central pyrenean hinterland, France). Tectonics 42, e2023TC007828. https://doi.org/10.1029/2023TC007828.
Chapman, J.B., DeCelles, P.G., 2015. Foreland basin stratigraphic control on thrust belt evolution. Geology 43, 579–582. https://doi.org/10.1130/G36597.1.
Cifelli, F., Mattei, M., Chadima, M., Hirt, A., Hansen, A., 2005. The origin of tectonic lineation in extensional basins: combined neutron texture and magnetic analyses on "undeformed" clays. Earth Planet Sci. Lett. 235, 62–78. https://doi.org/10.1016/j.epsl.2005.02.042.
Cifelli, F., Mattei, M., Hirt, A.M., Günther, A., 2004. The origin of tectonic fabrics in "undeformed" clays: the early stages of deformation in extensional sedimentary basins: origin of tectonic fabrics. Geophys. Res. Lett. 31 https://doi.org/10.1029/2004GL019609 n/a-n/a.
Dahlen, F.A., Suppe, J., Davis, D., 1984. Mechanics of fold-and-thrust belts and accretionary wedges: cohesive Coulomb Theory. J. Geophys. Res. 89, 10087–10101. https://doi.org/10.1029/JB089iB12p10087.
Davis, D., Suppe, J., Dahlen, F.A., 1983. Mechanics of fold-and-thrust belts and accretionary wedges. J. Geophys. Res. 88, 1153. https://doi.org/10.1029/JB088iB02p01153.
Davis, D.M., Engelder, T., 1985. The role of salt in fold-and-thrust belts. Tectonophysics 119, 67–88. https://doi.org/10.1016/0040-1951(85)90033-2.
DeCelles, P.G., Gehrels, G.E., Quade, J., Ojha, T.P., Kapp, P.A., Upreti, B.N., 1998. Neogene foreland basin deposits, erosional unroofing, and the kinematic history of the Himalayan fold-thrust belt, western Nepal. Geol. Soc. Am. Bull. 110, 2–21. https://doi.org/10.1130/0016-7606(1998)110<0002:NFBDEU>2.3.CO;2.
DeCelles, P.G., Giles, K.A., 1996. Foreland basin systems. Basin Res. 8, 105–123. https://doi.org/10.1046/j.1365-2117.1996.01491.x.
DeCelles, P.G., Robinson, D.M., Quade, J., Ojha, T.P., Garzione, C.N., Copeland, P., Upreti, B.N., 2001. Stratigraphy, structure, and tectonic evolution of the Himalayan fold-thrust belt in western Nepal. Tectonics 20, 487–509. https://doi.org/10.1029/2000TC001226.
Deville, E., Dutrannoy, C., Schmitz, J., Vincent, B., Kohler, E., Lahfid, A., 2020. Shale tectonic processes: field evidence from the Parras Basin (north-eastern Mexico). Mar. Petrol. Geol. 122, 104688 https://doi.org/10.1016/j.marpetgeo.2020.104688.
Duerto, L., McClay, K., 2011. Role of the shale tectonics on the evolution of the Eastern Venezuelan Cenozoic thrust and fold belt. Mar. Petrol. Geol. 28, 81–108. https://doi.org/10.1016/j.marpetgeo.2009.11.005.
Duerto, L., McClay, K., 2009. The role of syntectonic sedimentation in the evolution of doubly vergent thrust wedges and foreland folds. Mar. Petrol. Geol. 26, 1051–1069. https://doi.org/10.1016/j.marpetgeo.2008.07.004.
Fillon, C., Huismans, R.S., Van Der Beek, P., 2013. Syntectonic sedimentation effects on the growth of fold-and-thrust belts. Geology 41, 83–86. https://doi.org/10.1130/G33531.1.
Ford, M., Masini, E., Vergés, J., Pik, R., Ternois, S., Léger, J., Dielforder, A., Frasca, G., Grool, A., Vinciguerra, C., Bernard, T., Angrand, P., Crémades, A., Manatschal, G., Chevrot, S., Jolivet, L., Mouthereau, F., Thinon, I., Calassou, S., 2022. Evolution of a low convergence collisional orogen: a review of Pyrenean orogenesis. BSGF - Earth Sci. Bull 193, 19. https://doi.org/10.1051/bsgf/2022018.
Garcés, M., López-Blanco, M., Valero, L., Beamud, E., Muñoz, J.A., Oliva-Urcia, B., Vinyoles, A., Arbués, P., Cabello, P., Cabrera, L., 2020. Paleogeographic and sedimentary evolution of the South Pyrenean foreland basin. Mar. Petrol. Geol. 113, 104105 https://doi.org/10.1016/j.marpetgeo.2019.104105.
Gracia-Puzo, F., Aubourg, C., Casas-Sainz, A., 2021. A fast way to estimate the clay fabric from shale fragments. Key example from a strained thrust footwall (Pyrenees). J. Struct. Geol. 152, 104443 https://doi.org/10.1016/j.jsg.2021.104443.
Gupta, K.D., Pickering, K.T., 2008. Petrography and temporal changes in petrofacies of deep-marine Ainsa-Jaca basin sandstone systems, Early and Middle Eocene, Spanish Pyrenees: petrofacies of Eocene deep-marine Ainsa-Jaca basin. Sedimentology 55, 1083–1114. https://doi.org/10.1111/j.1365-3091.2007.00937.x.
Hogan, P.J., 1993. Geochronologic, Tectonic, and Stratigraphic Evolution of the Southwest Pyrenean Foreland Basin, Northern Spain. University of southern California.
Hogan, P.J., Burbank, D.W., 1996. Evolution of the Jaca piggyback basin and emergence of the external Sierra, southern Pyrenees. In: Friend, P.F., Dabrio, C.J. (Eds.), Tertiary Basins of Spain. Cambridge University Press, pp. 153–160. https://doi.org/10.1017/CBO9780511524851.023.
Hrouda, F., 1982. Magnetic anisotropy of rocks and its application in geology and geophysics. Geophys. Surv. 5, 37–82. https://doi.org/10.1007/BF01450244.
Hudec, M.R., Soto, J.I., 2021. Piercement mechanisms for mobile shales. Basin Res. 33, 2862–2882. https://doi.org/10.1111/bre.12586.
Jelínek, V., 1978. Statistical processing of anisotropy of magnetic susceptibility measured on groups of specimens. Studia Geophys. Geod. 22, 50–62. https://doi.org/10.1007/BF01613632.
Kergaravat, C., Ribes, C., Callot, J.-P., Ringenbach, J.-C., 2017. Tectono-stratigraphic evolution of salt-controlled minibasins in a fold and thrust belt, the Oligo-Miocene central Sivas Basin. J. Struct. Geol. 102, 75–97. https://doi.org/10.1016/j.jsg.2017.07.007.
Kissel, C., Barrier, E., Laj, C., Lee, T.-Q., 1986. Magnetic fabric in "undeformed" marine clays from compressional zones. Tectonics 5, 769–781. https://doi.org/10.1029/TC005i005p00769.
Labaume, P., Meresse, F., Jolivet, M., Teixell, A., Lahfid, A., 2016. Tectonothermal history of an exhumed thrust-sheet-top basin: an example from the south Pyrenean thrust belt: jaca thrust-sheet-top basin. Tectonics 35, 1280–1313. https://doi.org/10.1002/2016TC004192.
Labaume, P., Mutti, E., Seguret, M., 1987. Megaturbidites: a depositional model from the eocene of the SW-Pyrenean Foreland basin, Spain. Geo Mar. Lett. 7, 91–101. https://doi.org/10.1007/BF02237988.
Labaume, P., Séguret, M., Mutti, E., 1983. Mégaturbidites carbonatées du bassin turbiditique de l'Eocène inférieur et moyen sud-pyrénéen. Bull. Soc. Geol. Fr. 25, 927–941.
Labaume, P., Séguret, M., Seyve, C., 1985. Evolution of a turbiditic foreland basin and analogy with an accretionary prism: example of the Eocene South-Pyrenean Basin. Tectonics 4, 661–685. https://doi.org/10.1029/TC004i007p00661.
Labaume, P., Teixell, A., 2018. 3D structure of subsurface thrusts in the eastern Jaca Basin, southern Pyrenees. Geol. Acta 22.
Lacombe, O., Beaudoin, N.E., Hoareau, G., Labeur, A., Pecheyran, C., Callot, J.-P., 2021. Dating folding beyond folding, from layer-parallel shortening to fold tightening, using mesostructures: lessons from the Apennines, Pyrenees, and Rocky Mountains. Solid Earth 12, 2145–2157. https://doi.org/10.5194/se-12-2145-2021.
Lafargue, E., Marquis, F., Pillot, D., 1998. Rock-eval 6 applications in hydrocarbon exploration, production, and soil contamination studies. Rev. Inst. Fr. Pét. 53, 421–437. https://doi.org/10.2516/ogst:1998036.
Lago, M., Arranz, E., Pocoví, A., Galé, C., Gil-Imaz, A., 2004. Permian magmatism and basin dynamics in the southern Pyrenees: a record of the transition from late Variscan transtension to early Alpine extension. Geol. Soc. London, Spec. Public 223, 439–464. https://doi.org/10.1144/GSL.SP.2004.223.01.19.
Larrasoaña, J.C., Pueyo-Morer, E.L., Millán-Garrido, H., Parés, J.M., Del Valle, J., 1997. Deformation mechanisms deduced from AMS data in the Jaca-Pamplona basin (southern Pyrenees). Phys. Chem. Earth 22, 147–152. https://doi.org/10.1016/S0079-1946(97)00093-1.
Lartigau, M., Kergaravat, C., Callot, J.-P., Aubourg, C., Ringenbach, J.-C., 2023. Matrix deformation and fracture network in minibasins in a foreland fold and thrust belt: the Sivas Basin, Turkey. Tectonophysics 847, 229701. https://doi.org/10.1016/j.tecto.2022.229701.
Lloret, J., López-Gómez, J., Heredia, N., Martín-González, F., de la Horra, R., Borruel-Abadía, V., Ronchi, A., Barrenechea, J.F., García-Sansegundo, J., Galé, C., Ubide, T., Gretter, N., Diez, J.B., Juncal, M., Lago, M., 2021. Transition between variscan and

alpine cycles in the pyrenean-cantabrian mountains (N Spain): geodynamic evolution of near-equator European permian basins. Global Planet. Change 207, 103677. https://doi.org/10.1016/j.gloplacha.2021.103677.
Luzón, A., 2005. Oligocene–Miocene alluvial sedimentation in the northern Ebro Basin, NE Spain: tectonic control and palaeogeographical evolution. Sediment. Geol. 177, 19–39. https://doi.org/10.1016/j.sedgeo.2005.01.013.
McQuarrie, N., 2002. The kinematic history of the central Andean fold-thrust belt, Bolivia: implications for building a high plateau. Geol. Soc. Am. Bull. 114 (8), 950–963.
McQuarrie, N., DeCelles, P., 2001. Geometry and structural evolution of the central Andean backthrust belt, Bolivia. Tectonics 20, 669–692.
Millan Garrido, H., Aurell, M., Melendez, A., 1994. Synchronous detachment folds and coeval sedimentation in the Prepyrenean External Sierras (Spain): a case study for a tectonic origin of sequences and systems tracts. Sedimentology 41, 1001–1024. https://doi.org/10.1111/j.1365-3091.1994.tb01437.x.
Millan Garrido, H., Oliva-Urcia, B., Pocoví Juan, A., 2006. La transversal de Gavarnie-Guara. Estructura y edad de los mantos de Gavarnie, Guara-Gèdre y Guarga (Pirineo centro- Occidental). Geogaceta 40, 35–38.
Millan Garrido, H., Pueyo-Morer, E.L., Aurell Cardona, M., Luzón, A., Oliva-Urcia, B., Martinez, Pena, Pocoví Juan, A., 2000. Actividad tectonica depositos terciarios frente meridional del Pirineo central. Rev. Soc. Geol. Espana 13, 279–300.
Mochales, T., Barnolas, A., Pueyo, E.L., Serra-Kiel, J., Casas, A.M., Samso, J.M., Ramajo, J., Sanjuan, J., 2012. Chronostratigraphy of the boltana anticline and the ainsa basin (southern Pyrenees). Geol. Soc. Am. Bull. 124 (1), 1229–1250. https://doi.org/10.1130/B30418.
Mochales, T., Pueyo, E.L., Casas, A.M., Barnolas, A., 2016. Restoring paleomagnetic data in complex superposed folding settings: the Boltaña anticline (Southern Pyrenees). Tectonophysics 671, 281–298. https://doi.org/10.1016/j.tecto.2016.01.008.
Montes, M., Colombo, F., 1996. Análisis secuencial y correlación de los abanicos aluviales de Peña Oroel y la Sierra de Candas.(Eoceno superior. Cuenca Surpirenaica Central). Geogaceta 20, 76–79.
Montes Santiago, M.J.M., 2009. Estratigrafía del Eoceno-Oligoceno de la cuenca de Jaca: sinclinorio del Guarga, Coleccion de Estudios Altoaragoneses. Instituto de Estudios Altoaragoneses.
Morley, C.K., 2003. Mobile shale related deformation in large deltas developed on passive and active margins. Geol. Soc. London, Special Pub 216, 335–357.
Morley, C.K., Crevello, P., Ahmad, Z.H., 1998. Shale tectonics and deformation associated with active diapirism: the Jerudong Anticline, Brunei Darussalam. J. Geol. Soc. 155, 475–490. https://doi.org/10.1144/gsjgs.155.3.0475.
Morley, C.K., von Hagke, C., Hansberry, R., Collins, A., Kanitpanyacharoen, W., King, R., 2018. Review of major shale-dominated detachment and thrust characteristics in the diagenetic zone: Part II, rock mechanics and microscopic scale. Earth Sci. Rev. 176, 19–50. https://doi.org/10.1016/j.earscirev.2017.09.015.
Morley, C.K., von Hagke, C., Hansberry, R.L., Collins, A.S., Kanitpanyacharoen, W., King, R., 2017. Review of major shale-dominated detachment and thrust characteristics in the diagenetic zone: Part I, meso- and macro-scopic scale. Earth Sci. Rev. 173, 168–228. https://doi.org/10.1016/j.earscirev.2017.07.019.
Muñoz, J.-A., Beamud, E., Fernández, O., Arbués, P., Dinarès-Turell, J., Poblet, J., 2013. The Ainsa Fold and thrust oblique zone of the central Pyrenees: kinematics of a curved contractional system from paleomagnetic and structural data: paleomagnetism in S pyrenees. Tectonics 32, 1142–1175. https://doi.org/10.1002/tect.20070.
Nalpas, T., Gapais, D., Vergés, J., Barrier, L., Gestain, V., Leroux, G., et al., 2003. Effects of rate and nature of synkinematic sedimentation on the growth of compressive structures constrained by analogue models and field examples. Geol. Soc. Lond. Spec. Publ. 208 (1), 307–319.
Nichols, G.J., 1987. The structure and stratigraphy of the western external Sierras of the Pyrenees, northern Spain. Geol. J. 22, 245–259. https://doi.org/10.1002/gj.3350220307.
Oliva-Urcia, B., Beamud, E., Arenas, C., Pueyo, E.L., Garcés, M., Soto, R., Valero, L., Pérez-Rivarés, F.J., 2019. Dating the northern deposits of the Ebro foreland basin; implications for the kinematics of the SW Pyrenean front. Tectonophysics 765, 11–34. https://doi.org/10.1016/j.tecto.2019.05.007.
Oliva-Urcia, B., Beamud, E., Garcés, M., Arenas, C., Soto, R., Pueyo, E.L., Pardo, G., 2015. New magnetostratigraphic dating of the Palaeogene syntectonic sediments of the west-central Pyrenees: tectonostratigraphic implications. Geol. Soc. London, Special Pub 425, 107–128. https://doi.org/10.1144/SP425.5.
Oms, O., Dinarès-Turell, J., Remacha, E., 2003. Magnetic stratigraphy from deep clastic turbidites: an example from the eocene Hecho group (southern Pyrenees). Studia Geophys. Geod. 14.
Oms, O., Remacha Grau, E., 1992. Estratigrafía del abanico deltaico de Santa Orosia (Eoceno medio y superior de la cuenca de Jaca, Prov. de Huesca). Geogaceta 12, 72–74.
Ori, G.G., Friend, P.F., 1984. Sedimentary basins formed and carried piggyback on active thrust sheets. Geology 12, 475–478.
Parés, J.M., 2015. Sixty years of anisotropy of magnetic susceptibility in deformed sedimentary rocks. Front. Earth Sci. 3, 13.
Parés, J.M., 2004. How deformed are weakly deformed mudrocks? Insights from magnetic anisotropy. Geol. Soc. London, Special Pub 238, 191–203. https://doi.org/10.1144/GSL.SP.2004.238.01.13.
Parés, J.M., van der Pluijm, B.A., Dinarès-Turell, J., 1999. Evolution of magnetic fabrics during incipient deformation of mudrocks (Pyrenees, northern Spain). Tectonophysics 307, 1–14. https://doi.org/10.1016/S0040-1951(99)00115-8.
Payros, A., Pujalte, V., Orue-Etxebarria, X., 1999. The South Pyrenean Eocene carbonate megabreccias revisited: new interpretation based on evidence from the Pamplona Basin. Sediment. Geol. 125, 165–194. https://doi.org/10.1016/S0037-0738(99)00004-4.
Pichot, T., Nalpas, T., 2009. Influence of synkinematic sedimentation in a thrust system with two decollement levels; analogue modelling. Tectonophysics 473 (3–4), 466–475.
Pocoví Juan, A., Pueyo Anchuela, Ó., Pueyo, E.L., Casas-Sainz, A.M., Román Berdiel, M. T., Gil Imaz, A., Ramajo Cordero, J., Mochales, T., García Lasanta, C., Izquierdo-Llavall, E., Parés, J.M., Sánchez, E., Soto Marín, R., Oliván, C., Rodríguez Pintó, A., Oliva-Urcia, B., Villalaín, J.J., 2014. Magnetic fabrics in the western central-pyrenees: an overview. Tectonophysics 629, 303–318. https://doi.org/10.1016/j.tecto.2014.03.027.
Pueyo Anchuela, Ó., Gil Imaz, A., Pocoví Juan, A., 2012a. Factors affecting the record of strain fabrics at the anisotropy of magnetic susceptibility: west-Central South-Pyrenean cleavage domain (Southern Pyrenees; NE Spain). Tectonophysics 554–557, 1–17. https://doi.org/10.1016/j.tecto.2012.05.028.
Pueyo Anchuela, Ó., Imaz, A.G., Juan, A.P., 2010. Significance of AMS in multilayer systems in fold-and-thrust belts. A case study from the Eocene turbidites in the southern Pyrenees (Spain). Geol. J. 45, 544–561. https://doi.org/10.1002/gj.1194.
Pueyo Anchuela, Ó., Imaz, A.G., Juan, A.P., Lloréns, J.F.I., 2011. Acquisition and blocking of magnetic fabrics in synsedimentary structures, Eocene Pyrenees, Spain: magnetic fabrics in synsedimentary structures. Geophys. J. Int. 186, 1015–1028. https://doi.org/10.1111/j.1365-246X.2011.05136.x.
Pueyo Anchuela, Ó., Pueyo, E.L., Pocoví Juan, A., Gil Imaz, A., 2012b. Vertical axis rotations in fold and thrust belts: comparison of AMS and paleomagnetic data in the western external Sierras (southern Pyrenees). Tectonophysics 532–535, 119–133. https://doi.org/10.1016/j.tecto.2012.01.023.
Pueyo-Morer, E.L., Millan-Garrido, H., Pocovi-Juan, A., Parés, J.M., 1997. Determination of the Folding Mechanism by AMS Data. Study of the Relation Between Shortening and Magnetic Anisotropy in the Pico del Aguila Anticline (Southern Pyrenees). Phys. Chem. Earth 22, 1995–201.
Puigdefábregas, C., 1975. La sedimentación molásica en la cuenca de Jaca, Monografias del instituto de estudios pirenaicos. CSIC-Instituto de Estudios Pirenaicos, Jaca.
Puigdefabregas, C., Souquet, P., 1986. Tecto-sedimentary cycles and depositional sequences of the mesozoic and tertiary from the Pyrenees. Tectonophysics 129, 173–203.
Remacha, E., Fernández, L.P., 2003. High-resolution correlation patterns in the turbidite systems of the Hecho group (South-Central Pyrenees, Spain). Mar. Petrol. Geol. 20, 711–726. https://doi.org/10.1016/j.marpetgeo.2003.09.003.
Remacha, E., Fernandez, L.P., Maestro, E., Oms, O., Estrada, R., Teixell, A., 1998. The Upper Hecho Group Turbidites and Their Vertical Evolution to Deltas (Eocene, South-Central Pyrenees).
Remacha, E., Oms, O., Coello, J., 1995. The Rapitán turbidite channel and its related eastern levee-overbank deposits, Eocene Hecho group, south-central Pyrenees, Spain. In: Pickering, K.T., Hiscott, R.N., Kenyon, N.H., Ricci Lucchi, F., Smith, R.D.A. (Eds.), Atlas of Deep Water Environments. Springer, Netherlands, Dordrecht, pp. 145–149. https://doi.org/10.1007/978-94-011-1234-5_22.
Rochette, P., Jackson, M., Aubourg, C., 1992. Rock magnetism and the interpretation of anisotropy of magnetic susceptibility. Rev. Geophys. 30.
Rodríguez-Méndez, L., Cuevas, J., Esteban, J.J., Tubía, J.M., Sergeev, S., Larionov, A., 2014. Age of the magmatism related to the inverted Stephanian–Permian basin of the Sallent area (Pyrenees). Geol. Soc. London, Special Pub 394, 101–111. https://doi.org/10.1144/SP394.2.
Rodríguez-Méndez, L., Cuevas, J., Tubía, J.M., 2016. Post-variscan basin evolution in the central Pyrenees: insights from the stephanian–permian anayet basin. Comptes rendus. Geoscience 348, 333–341. https://doi.org/10.1016/j.crte.2015.11.006.
Rodríguez-Pintó, A., Pueyo, E.L., Serra-Kiel, J., Samsó, J.M., Barnolas, A., Pocoví, A., 2012. Lutetian magnetostratigraphic calibration of larger foraminifera zonation (SBZ) in the Southern Pyrenees: the Isuela section. Palaeogeogr. Palaeoclimatol. Palaeoecol. 333–334, 107–120. https://doi.org/10.1016/j.palaeo.2012.03.012.
Roigé, M., Gómez-Gras, D., Remacha, E., Boya, S., Viaplana-Muzas, M., Teixell, A., 2017. Recycling an uplifted early foreland basin fill: an example from the Jaca basin (Southern Pyrenees, Spain). Sediment. Geol. 360, 1–21. https://doi.org/10.1016/j.sedgeo.2017.08.007.
Roigé, M., Gómez-Gras, D., Remacha, E., Daza, R., Boya, S., 2016. Tectonic control on sediment sources in the Jaca basin (middle and upper eocene of the South-central Pyrenees). Compt. Rendus Geosci. 348, 236–245. https://doi.org/10.1016/j.crte.2015.10.005.
Saur, H., Sénéchal, P., Boiron, T., Aubourg, C., Derluyn, H., Moonen, P., 2020. First investigation of quartz and calcite shape fabrics in strained shales by means of X-ray tomography. J. Struct. Geol. 130, 103905 https://doi.org/10.1016/j.jsg.2019.103905.
Soto, J.I., Fernandez-Ibanez, F., Talukder, A.R., Martinez-Garcia, P., 2010. Miocene shale tectonics in the northern alboran sea (western mediterranean). AAPG Memoir 93, 119–144. https://doi.org/10.1306/13231312M933422.
Soto, J.I., Heidari, M., Hudec, M.R., 2021a. Proposal for a mechanical model of mobile shales. Sci. Rep. 11, 23785 https://doi.org/10.1038/s41598-021-02868-x.
Soto, J.I., Hudec, M.R., 2023. Mud volcanoes guided by thrusting in compressional settings. Geology. https://doi.org/10.1130/G51235.1.
Soto, J.I., Hudec, M.R., Mondol, N.H., Heidari, M., 2021b. Shale transformations and physical properties—implications for seismic expression of mobile shales. Earth Sci. Rev. 220, 23.
Tarling, D., Hrouda, F., 1993. Magnetic Anisotropy of Rocks. Springer Science & Business Media.
Tavani, S., Storti, F., Lacombe, O., Corradetti, A., Muñoz, J.A., Mazzoli, S., 2015. A review of deformation pattern templates in foreland basin systems and fold-and-

thrust belts: implications for the state of stress in the frontal regions of thrust wedges. Earth Sci. Rev. 141, 82–104. https://doi.org/10.1016/j.earscirev.2014.11.013.
Teixell, A., 1996. The Ansó transect of the southern Pyrenees: basement and cover thrust geometries. J. Geol. Soc. 153, 301–310. https://doi.org/10.1144/gsjgs.153.2.0301.
Teixell, A., Labaume, P., Lagabrielle, Y., 2016. The crustal evolution of the west-central Pyrenees revisited: inferences from a new kinematic scenario. Comptes Rendus. Géoscience 348 (3–4), 257–267.
Vergés, J., Fernàndez, M., Martìnez, A., 2002. The Pyrenean orogen: pre-, syn-, and post-collisional evolution. J.Virt.Ex 08. https://doi.org/10.3809/jvirtex.2002.00058.
Vinyoles, A., López-Blanco, M., Garcés, M., Arbués, P., Valero, L., Beamud, E., et al., 2021. 10 Myr evolution of sedimentation rates in a deep marine to non-marine foreland basin system: Tectonic and sedimentary controls (Eocene, Tremp–Jaca Basin, Southern Pyrenees, NE Spain). Basin Res. 33 (1), 447–477.